

Experiments seepage reducing measures canal bed

Column tests and CST permeability tests



Experiments seepage reducing measures canal bed
Column tests and CST permeability tests

Author(s)

Lynrd de Wit

Qilong Bi

Experiments seepage reducing measures canal bed

Column tests and CST permeability tests

Client	Rijkswaterstaat Water, Verkeer en Leefomgeving
Contact	Roel Brugman
Projectreference	INF14 Maatregelen ter reductie wateroverlast langs kanalen
Keywords	Sand-bentonite, clay, mud, granulite, ZBM, zand-bentoniet, klei, slib, granuliet, Amsterdam-Rijnkanaal

Document control

Version	1.0
Date	27-03-2026
Project nr.	11211511-033
Document ID	11211511-033-GEO-0005
Pages	66
Classification	
Status	Final

Author(s)

	Lynyrd de Wit Qilong Bi	

The allowed use of this table is limited to check the correct order-performance by Deltares. Any other client-internal-use and any external distribution is not allowed.

Doc. version	Author	Reviewer	Approver
1.0	Lynyrd de Wit	Thijs van Kessel	Aukje Baaijens

Summary

This report is a product within sub-project 3.1 Measures of SITO-PS study "Measures to Reduce Seepage Issues Along Canals (ARK)", which uses the Amsterdam-Rhine Canal (ARK in Dutch) between Breukelen and Nigtevecht as a case study. The surrounding area experiences significant seepage and other excess water problems, linked to soil rupture and groundwater boils in the polders along the canal. This report describes an experimental investigation into "soft solutions" aimed at reducing water seepage along the Amsterdam-Rhine Canal near Nigtevecht. The research evaluates the effectiveness and durability of various sealing materials in reducing the permeability of the canal bed under dynamic conditions. The testing followed a two-phase approach:

- Capillary Suction Time (CST) tests: Small-scale static tests used to characterize the intrinsic permeability of material "recipes" and determine optimal sand-to-additive ratios.
- Column tests with dynamic loading: Larger-scale tests (1.5 m pressure head) utilizing a rotating vane to mimic the hydrodynamic shear stresses (0.6 to 2.4 m/s) induced by passing ships.

Five primary materials were evaluated in various mixtures and configurations: RONA ZBM (sand-bentonite mixture), OCMA bentonite, S1 clay, natural dredged mud, and granulite (Greenbase). The highest vane speed of 2.4 m/s in the column tests is 1.7x higher than the highest measured ship-induced flow velocity, but the corresponding bed shear stress from the vane corresponds to the highest measured shear stress in the 9-day field campaign in ARK (Deltares 2025a). Given the limited measurement period of 9 days in the field campaign it is possible that incidentally higher ship-induced flow speeds occur in the ARK. The occurrence of the high shear stresses in the vane protocol is more frequent than in the field measurements. Hence, the applied vane protocol is considered to be representative, but on the conservative side for ARK conditions.

The experimental investigations revealed a distinct performance hierarchy where sodium-activated bentonite outperforms clay, mud, and granulite due to active swelling properties that require significantly less material mass for effective sealing. When subjected to dynamic ship-induced shear, these materials typically followed a three-phase behavioral pattern involving initial consolidation, stepwise erosion during peak 2.4 m/s flow events, and subsequent stabilization. Although the hydrodynamic stress often erodes away the bulk of the initial capping layer, the system's long-term sealing capacity was maintained by a thin, robust "effective layer" that formed at the base interface and was continuously reinforced by the "self-healing" deposition of suspended fines. The durability of this seal was much improved by protective configurations; specifically, "sandwiching" pure clay or mud beneath a 30 cm sand layer increased resistance times to 80–90 days compared to just ~10 days for unprotected ZBM (for ZBM the 30 cm sand cover provided temporary improvement, but not towards the end of the test at which moment the resistance time also was ~10 days – similar to unprotected ZBM), while a gravel armor layer on top of ZBM yielded the highest observed resistance of ~221 days. For practical application in the ARK, these findings underscore the advantage of applying a protective overburden (sand or gravel) to dampen forces and ensuring a "resting time" to allow consolidation before exposure to heavy shipping traffic starts.

The report recommends further research into placement procedures (e.g., jetting or flume tests), the influence of background currents, and the impact of different sand cover thicknesses. A field pilot in the ARK is strongly advised to monitor in-situ erosion, deposition, and spatial redistribution of these materials over time.

Contents

	Summary	4
	Contents	5
1	Introduction	7
2	Solutions and materials	9
2.1	Tested soft solutions	9
2.2	Details of selected materials	12
2.2.1	ZBM Top Layer	12
2.2.2	OCMA Bentonitic Clay	12
2.2.3	Granulite	12
2.2.4	Clay	12
2.2.5	Dredged mud	12
2.2.6	Sand base layer	13
3	Experimental setup	14
3.1	Introduction of testing approaches	14
3.2	Capillary Suction Time (CST) tests	14
3.3	Column tests with dynamic loadings	16
3.3.1	The setup of the column	16
3.3.2	The protocol for vane operation	17
3.3.3	The preparation of the test	20
3.3.4	Interpretation of the results	20
4	Results	21
4.1	Results CST tests	21
4.1.1	Reference case	21
4.1.2	Results of sand-material mixtures	21
4.1.3	Results of pure clay and pure dredged mud	25
4.1.4	Overview of the tested recipes	27
4.2	Results column tests with vane	27
4.2.1	ZBM test results (solutions applied in the Twentekanaal)	28
4.2.2	Sand – OCMA bentonite test results (soft solution with 40 cm layer)	31
4.2.3	Sand – S1 clay test results (soft solution with 40 cm layer)	34
4.2.4	Sand – dredged mud test results (soft solution with 40 cm layer)	37
4.2.5	Sand – granulite test results (soft solution with 40 cm layer)	40
4.2.6	Materials with a protection sand layer on top	43
4.2.7	ZBM with a protection gravel layer on top	47
5	Discussions and conclusions	50
5.1	Mechanisms of sealing and performance grading from the CST tests	50
5.2	Overview of the column test results	51
5.3	General behaviour of soft solutions under dynamic loading in the column tests	53

5.4	Reflections on test setup	54
5.5	Practical conclusions for ARK	55
6	Recommendations	57
7	References	58
A	Appendix	61
A.1	Column test data postprocessing	61
A.2	Sand – OCMA bentonite CST tests results	61
A.3	Sand – S1 clay CST test results	62
A.4	Sand – dredged mud CST test results	63
A.5	Sand – granulite CST test results	64

1 Introduction

Deltares conducts research within the infrastructure domain to develop solutions for challenges related to new infrastructure and the maintenance and preservation of existing infrastructure. One of the challenges is the widening and/or deepening of canals to accommodate more traffic and larger vessels. Limited space along canals and the environmental impact of widening or deepening can pose significant constraints.

Modifications to canals can increase environmental impacts, for example through seepage, particularly when the canal is situated higher than the surrounding land. Canal managers need a clear understanding of potential improvement measures (including reducing seepage) and their implications in order to make well-informed decisions. This is the focus of the SITO-PS study “Maatregelen ter reductie wateroverlast langs kanalen (ARK)” (“Measures to Reduce Seepage Issues Along Canals (ARK)”), which uses the Amsterdam-Rhine Canal (ARK in Dutch) between Breukelen and Nigtevecht as a case study. Figure 1-1 shows a schematic of the ARK water system. The surrounding area experiences significant seepage and other excess water problems, linked to soil rupture and groundwater boils in the polders along the canal. Figure 1-2 shows the location of these groundwater boils identified by Waternet.

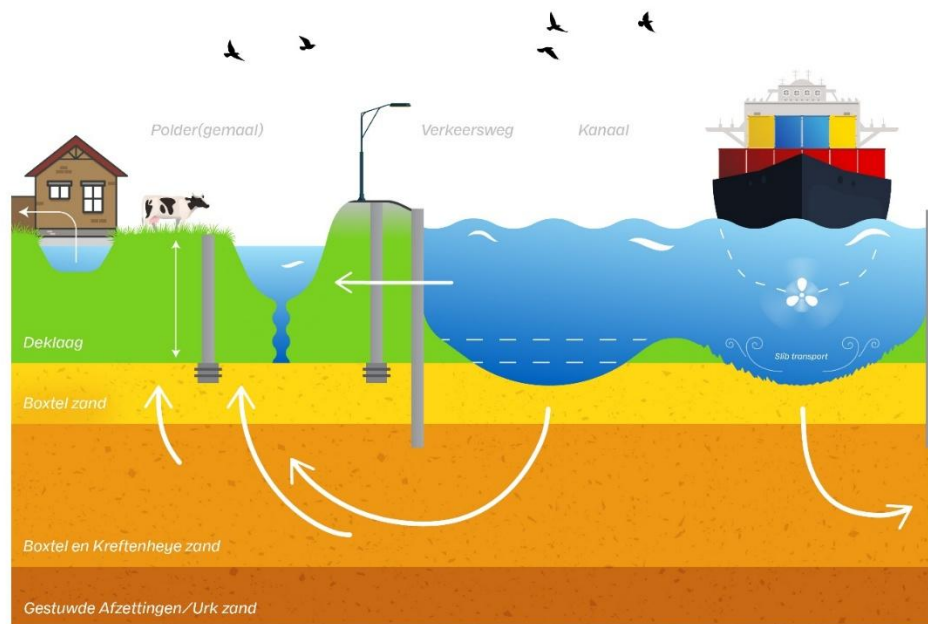


Figure 1-1. Schematic of the water system of the ARK

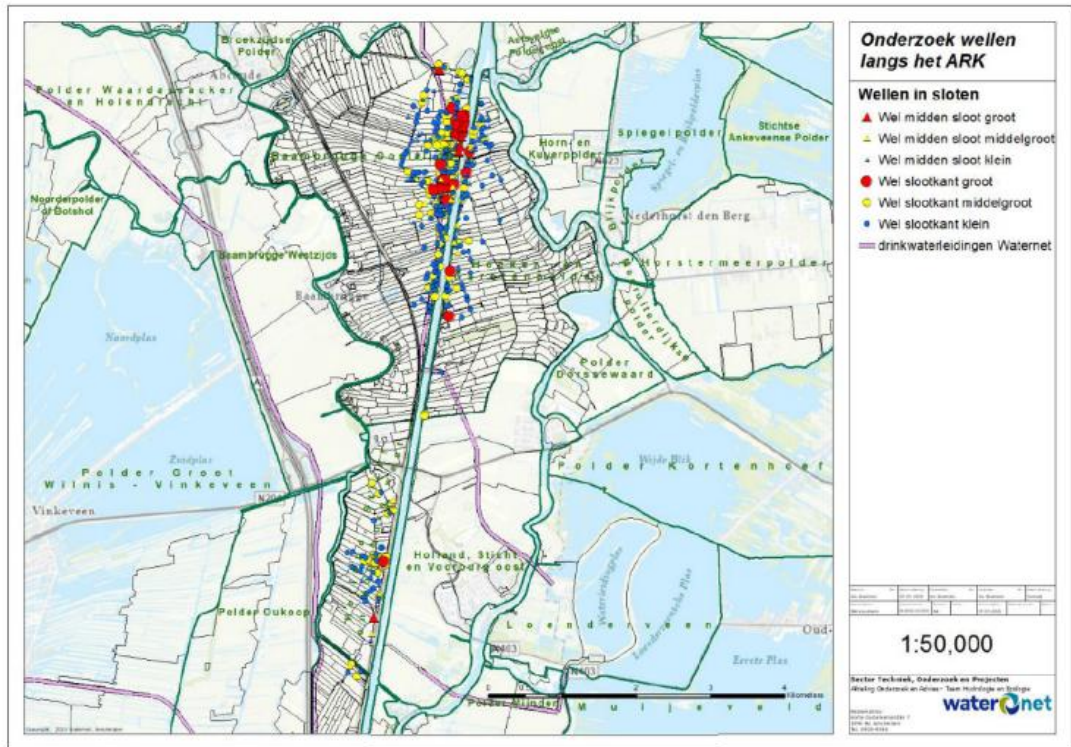


Figure 1-2. Overview of ARK groundwater boils in near Nigtevecht

This report is a product within sub-project 3.1 Measures. It describes a concise series of experimental tests of potential soft solutions to make the canal bed less permeable. The tested potential soft solutions consist of capping the canal bed with a layer of bentonite, granulite (Greenbase), clay and dredged mud in different ratios mixed with sand.

In Chapter 2 the selection of the capping material is discussed. Next, in Chapter 3 the two experimental setups are discussed. The first setup is a small-scale Capillary Suction Test (CST) permeability test to find the proper recipes to be tested in the subsequent column tests. The second setup is a larger-scale column test in which a sand layer is placed with a certain soft solution on top to mimic the canal bed. A pressure head of 1.5 m, similar to the pressure head at ARK, is applied in the test and the amount of water seeping through the sediment bed is measured over time. Periodically a vane exerts a rotating flow to mimic the stirring behaviour of ship passages. In Chapter 4 the results of both test series are presented. In Chapter 5 these results are discussed and conclusions are drawn. Finally, recommendations are made in Chapter 6.

2 Solutions and materials

2.1 Tested soft solutions

The test program focusses on solutions to make a canal bed less permeable. The tests investigate the effectiveness of a certain solution in reducing the permeability, and how the permeability changes after periodic shear from a vane which mimics the effect of passing ships. Making a canal bed less permeable can be achieved in different manners, see also Deltares (2024), for example by:

- a) Sealing the canal with a foil, textile or mattress (for example Sibelonmat, bentonite mattress).
- b) Soil improvement by injection. This can be achieved by for example bio-degradable Xanthan Gum (Rehman Lund (2024), Deltares (2022)) or non bio-degradable LAPAM (Linear Anionic PolyAcrylaMide) (Rehman Lund (2021) or with geochemical reactive substances like Soseal or iron ore (ijzeroer) which can clog the pores of the sand matrix by a chemical reaction.
- c) Placing a layer of fine sediment with low permeability.

Option a) is not tested in this program because no knowledge gaps exists about the sealing properties of those types of solutions. Option b) is not included in this program because geochemical substances are (so far) only used in stagnant water systems. Its effectiveness for a highly dynamic bed with continuous stirring from ships is highly uncertain. Additionally, the standard placement method of injecting via spray lances is not suitable for a busy canal like ARK. Xanthan Gum (XG) and LAPAM are not tested as they degrade and require periodic reapplication. Additionally, for XG there is the concern about the unknown ecological effects on algae and other biota (XG is an eatable polysaccharide) and for LAPAM there is a concern about the potential negative ecological effects of the degradation of polyacrylamide into monomers.

Therefore, the test program focusses on potential solutions of option c). In the test program the following soils are being tested for different layer thicknesses and ratios with sand:

- Pre-mixed RONA ZBM (sand-bentonite mixture)
- OCMA bentonite
- Granulite (Greenbase)
- Clay (S1)
- Natural dredged mud from Hollandse IJssel

Figure 2-1 shows the tested materials. The details about the different materials are described in §2.2. The test matrix of the different solutions and layer compositions tested in the column tests can be found in Table 2-1. The rationale of the tests is explained below.

Application of 10 cm RONA ZBM in the Twentekanaal functions as bottom-sealant (Rijkswaterstaat 2022, Rijkswaterstaat 2024). In 2019 (Deltares 2019a) column tests have been conducted with 5 cm (60 kg/m² ZBM) and 10 cm ZBM (120 kg/m² ZBM), where the 5 cm test included vane action with a different protocol as used in the 2025 tests and 10 cm ZBM is not tested with vane action. In the 2025 column tests pre-mixed RONA ZBM is tested with 4 cm (51 kg/m²) and 8 cm (102 kg/m²) layers to get more insight into the influence of the layer thickness on the resistance against periodic hydrodynamic loads from the vane. The effective amount of ZBM in kg/m² in the 2025 column tests is slightly less than in the 2019 column tests because of differences in placement method and ZBM mixture density as delivered by van Heteren. In 2019 some dilution occurred during placement via a tube and in 2025 the ZBM is

placed undiluted on top of the sand. For OCMA bentonite, granulite, clay, and natural dredged mud, tests are performed with a 40 cm thick mixture with two ratios of sand-to-tested material: a rich mixture with lower permeability and a poorer mixture with higher permeability. Because one test with a mixture of sand and dredged mud failed due to clogging of an outlet tube, this mixture is only tested for one ratio of sand-dredged-mud. Additionally, tests are performed with 8 cm RONA ZBM, 10 cm S1 clay or 10 cm dredged mud covered with 30 cm sand and 8 cm RONA ZBM covered with a layer of gravel. It is investigated whether the sand or gravel on top of a soft solution functions as extra protection against erosion.

The tests of the different soft solutions provide insight whether their sealing behaviour and erosion resistance is comparable and how much material is needed to achieve a certain reduction in permeability. The rich and poor mixtures provide insight how the reduction of permeability and resistance to the periodic hydrodynamic loads depends on the recipe of each soft solution. A thin layer of clay or dredged mud is only investigated with 30 cm of sand on top, as it is anticipated that a thin layer of pure clay or dredged mud without sand cover will not perform better than a thin layer of ZBM. ZBM has the advantage of the active swelling behavior of bentonite and has proven its functioning in the Twentekanaal and in earlier tests. Technically, a thin layer of pure granulite may also be a possibility, but we cannot test this with the present setup. In 2019 (Deltares 2019a) it was found that water is leaking at the interface granulite-plexiglass which influenced the results significantly.

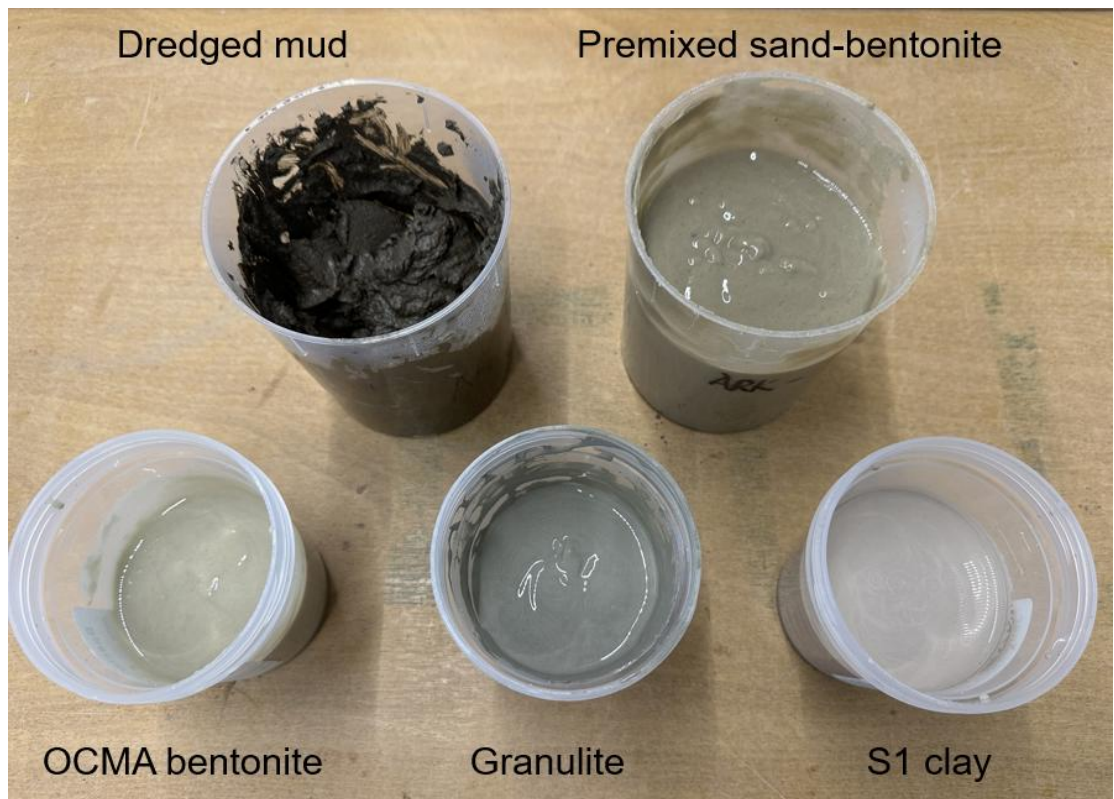


Figure 2-1. Tested soft solutions

Table 2-1. Tested soft solutions layer compositions in column tests

#	Description	Layer construction
1	ZBM double layer 8 cm (comparable to Twentekanaal tests 2019)	30 cm sand + 8 cm ZBM (102 kg/m ²)
2	ZBM thin layer 4 cm (comparable to Twentekanaal tests 2019)	30 cm sand + 4 cm ZBM (51 kg/m ²)
3	Soil improvement with homogeneous sand-bentonite mixture with high concentration of OCMA bentonite ¹ (but lower concentration than a pure ZBM layer)	30 cm sand + 40 cm sand-bentonite mixture
4	Soil improvement with homogeneous sand-bentonite mixture with low concentration of OCMA bentonite ²	30 cm sand + 40 cm sand-bentonite mixture
5	Soil improvement with homogeneous sand-clay mixture with high concentration of S1 clay ¹	30 cm sand + 40 cm sand-clay mixture
6	Soil improvement with homogeneous sand-clay mixture with low concentration of S1 clay ²	30 cm sand + 40 cm sand-clay mixture
7	Soil improvement with homogeneous sand-dredged material mixture with high concentration of dredged material ¹	30 cm sand + 40 cm sand-dredged mud mixture
8	Soil improvement with homogeneous sand-dredged material mixture with low concentration of dredged material ²	30 cm sand + 40 cm sand-dredged mud mixture
9	Soil improvement with homogeneous sand-granulite mixture with high concentration of granulite ¹	30 cm sand + 40 cm sand-granulite mixture
10	Soil improvement with homogeneous sand-granulite mixture with low concentration of granulite ²	30 cm sand + 40 cm sand-granulite mixture
11	8 cm ZBM with 30 cm sand on top	30 cm sand + 8 cm ZBM + 30 cm sand
12	10 cm clay with 30 cm sand on top	30 cm sand + 10 cm clay + 30 cm sand

¹ Concentration leading to a mixture hydraulic conductivity (k_v) of $\sim 0.5 \cdot 10^{-7}$ m/s (0.4 m then provides 88 days resistance); to be determined via rapid filtration CST test.

² Concentration leading to a mixture hydraulic conductivity (k_v) of $\sim 1.0 \cdot 10^{-7}$ m/s (0.4 m then provides 44 days resistance); to be determined via rapid filtration CST test.

#	Description	Layer construction
13	10 cm dredged material with 30 cm sand on top	30 cm sand + 10 cm dredged mud + 30 cm sand
14	8 cm ZBM with gravel layer on top as extra protection against ship loading	30 cm sand + 8 cm ZBM + 10 cm gravel

2.2 Details of selected materials

2.2.1 ZBM Top Layer

For the tests involving a ZBM top layer, Van Heteren is acknowledged for supplying RONA ZBM mixture. This mixture has also been used for sealing the Twentekanaal.

2.2.2 OCMA Bentonitic Clay

For the bentonitic clay, Cebogel OCMA is used, a sodium-activated bentonite. This product is comparable to the bentonite used by Van Heteren to generate RONA ZBM. An alternative option is calcium-activated bentonite; however, this would require approximately five times more material to achieve similar performance (Deltares, 2020).

2.2.3 Granulite

Bontrup is acknowledged for supplying Greenseal (granulite) for the tests.

2.2.4 Clay

Sibelco FT-S1 clay is used. The material has the following characteristics:

- Particle size distribution: 83% < 2 µm; 99% < 63 µm.
- Mineralogy: 64% kaolinite group minerals, 10% sericite/illite, 19% quartz.

2.2.5 Dredged mud

For the eventual application in the ARK, locally sourced dredged material may have an advantage for being circular and for CO₂ and costs reductions. Within the testing programme, the objective is to use dredged material with comparable geotechnical and sedimentary properties.

Certain sources are considered less suitable:

- Loosdrechtse Plassen: material is highly peat-rich and very soft.
- Port of Amsterdam: material is frequently classified as industrial grade.
- Port of Rotterdam: material originates from saline or brackish conditions and is located farther from the project site.

Since the ARK is a freshwater system, the dredged material used in the tests must also originate from a freshwater environment, as flocculation behaviour differs significantly between saline and freshwater sediments. A further preference is given to mechanically dredged material brought above water level, ensuring a low initial water content. Adding water for experimental purposes is straightforward, whereas removing water through settling and consolidation is time-consuming.

No ongoing freshwater dredging project was identified and therefore mud deposited along the foreshore of the Hollandse IJssel dike near Gouda was collected for the tests.

2.2.6 Sand base layer

The bottom 30 cm of the column, below each tested solution, is filled with Sibelco S90 sand with the following characteristics:

- d_{50} : 149–184 μm
- d_{10} : 101–131 μm

Comparative data from in-situ measurements:

- Samples collected from sand beneath the Holocene cover layer of the ARK (Geolab Wiertsema, 2025; Deltares 2025b):
 - d_{50} : 139–295 μm (average 167 μm)
 - d_{10} : 71–189 μm (average 95 μm)
- DINO Loket³ data for the ARK near Nigtevecht:
 - d_{50} : 180–200 μm
 - d_{10} : 100–120 μm
- Grab samples taken from the top few centimeters of the ARK canal 500-1000 m south of Nigtevecht (Deltares 2025a):
 - d_{50} : 170-210 μm (average 183 μm)
 - d_{10} : 110–140 μm (average 121 μm)

Based on these values, Sibelco S90 sand closely matches the particle-size characteristics of the native sand layer in the ARK subsurface and is therefore considered a suitable reference material for the testing programme.

³ The DINO-loket (Data en Informatie van de Nederlandse Ondergrond) is a platform of TNO where Dutch soil data is collected and made available.

3 Experimental setup

3.1 Introduction of testing approaches

The experimental program in this study evaluates the efficacy of "soft" sealing solutions, specifically sediment mixtures composed of sand mixed with bentonite, granulite, clay, or natural mud. To provide a comprehensive assessment of these materials—ranging from their intrinsic material properties to their behaviour under operational stress—the study employs a two-phase experimental approach consisting of Capillary Suction Time (CST) tests and Column tests with dynamic loadings.

The initial phase utilizes the Capillary Suction Time (CST) test to characterize the fundamental permeability of the various sediment mixtures. This method allows for the estimation of hydraulic conductivity by measuring the suction time of water diffusing through a sample in a standard apparatus. The primary objectives of the CST phase are:

- **Baseline Assessment:** To determine the permeability of materials in a homogenous, undamaged condition.
- **Recipe Formulation:** To function as a screening tool for "finding the good recipes," effectively determining the optimal ratios of sand-to-tested material (e.g., determining the volumetric concentration of bentonite or clay per volume of water in the mixture).

These static tests provide the necessary baseline data to select the most promising mixture configurations for further testing. While CST tests establish intrinsic material properties, they cannot account for the physical degradation caused by ship traffic. To address this, the second phase involves column tests designed to subject the sediment recipes to dynamic shear stress. The specific characteristics of the column tests include:

- **Simulation of ship action:** A programmable rotating vane is utilized within the column to generate shear stress, mimicking the hydraulic forces exerted by passing ships. The protocol simulates realistic traffic, including varying speeds (0.6 m/s to 2.4 m/s) and rest periods, representative of moments in between passing ships.
- **Complex layering:** Unlike the homogenous samples in CST, the column tests evaluate complex stratigraphy, such as a base sand layer topped with a mixture layer, or "sandwich" configurations (sand-mixture-sand).
- **Dynamic permeability:** The test measures the mass of water leakage over time while the bed is subjected to mechanical agitation, allowing for the observation of erosion, crack development, and self-repairing mechanisms under load.

By integrating these two methods, the study links the theoretical permeability of specific material "recipes" derived from CST data to their stability when exposed to periodic hydrodynamic forces simulated in the Column tests. The two types of experiments are discussed in detail in the following sections.

3.2 Capillary Suction Time (CST) tests

The Capillary Suction Time (CST) test functions as a rapid laboratory technique designed to estimate the hydraulic conductivity of sediment mixtures in a static, baseline state. The test utilizes a standard apparatus consisting of a central reservoir placed upon a filter medium held by two vertically stacked plastic plates.

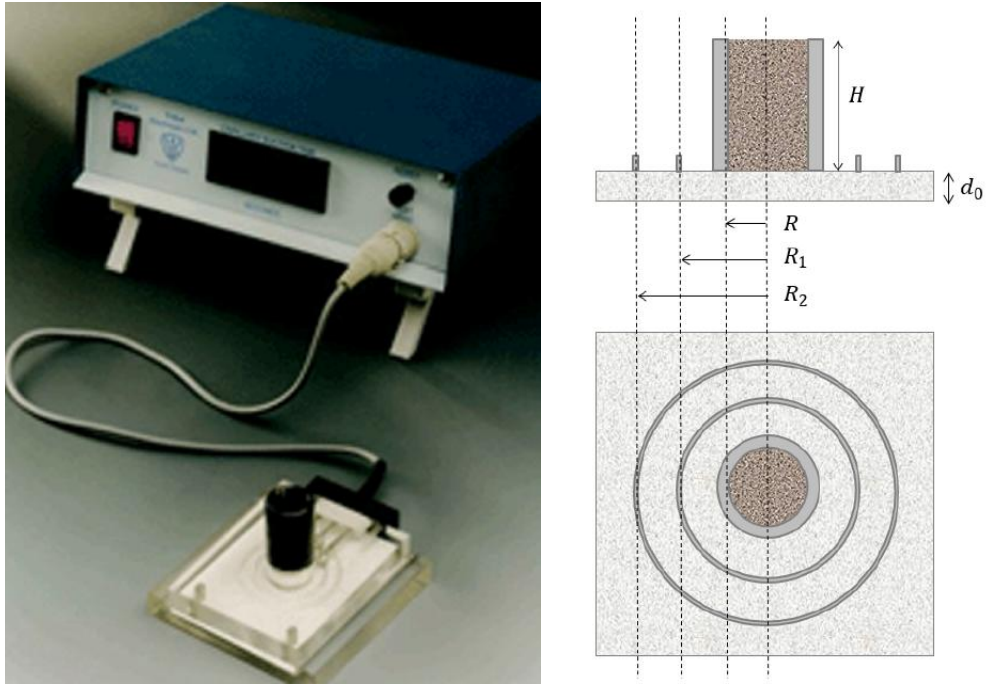


Figure 3-1. The standard type 304 Capillary Suction Time (CST) apparatus manufactured by Triton Electronics Ltd (left, from Gray, 2015), and principle of CST (right, from Chassagne and van Kan, 2023).

The working principle relies on the capillary suction pressure of the filter paper to draw water out of the sample mixture (Figure 3-1). The capillary suction pressure generated by standard filter paper (~ 7.5 kPa) is used to 'suck' water from the sample. The rate at which water permeates through the filter paper varies depending on the condition of the material and the filterability of the cake formed on the filter paper. CST is obtained from two electrodes placed at a standard interval ($R_2 - R_1$) between the inner ring and the outer ring from the cylindrical reservoir with a defined height (H) and radius (R). The time taken for the water front to pass between these two electrodes is recorded and considered as the CST (Triton Electronics Ltd, 2025). The force generated by capillary suction is much greater than the hydrostatic head within the funnel, so the pressure gradient driving the flow is determined primarily by the sample height.

While the direct output of the device is a time value (measured in seconds), the test effectively measures the mixture's permeability or hydraulic conductivity in a homogenous, undamaged condition. By integrating the measured suction time with the specific geometry of the reservoir, the permeability (hydraulic conductivity) of the sample mixture can be mathematically calculated by establishing a mass balance between the vertical outflow from the central cylinder and the radial absorption into the surrounding filter paper (Chassagne and van Kan, 2023; Talmon, 2026). The key idea is to equate the flow rate leaving the cylinder (driven by suction pressure according to Darcy's law) with the volumetric filling rate of the paper's pore space. The formulation from Talmon (2026) is used in this study. It states that the capillary suction time is non-linearly dependent on the radial distance between R_1 and R_2 in the filter paper as water spreads outward into a ring:

$$k = \mu H \frac{\phi_{paper}}{P_{capi}} \frac{d_0 (R_1 + R_2)}{R^2} \frac{R_2 - R_1}{\Delta t} \quad (1)$$

where k is the permeability of the sample (m^2), μ is the dynamic viscosity of water ($Pa \cdot s$), H is the height of the sample (m), ϕ_{paper} is the porosity of the filter paper (-), P_{capi} is the capillary suction pressure (Pa) exerted at the bottom of the sample by the filter paper, R , R_1 and R_2 are

the radius of the cylinder, inner and the outer rings (m) respectively, d_0 is the thickness of the filter paper (m), and Δt is the measured time. In this study, the geometric parameters are known from the apparatus, of which $H = 1.8 \text{ cm}$, $R = 0.9 \text{ cm}$, $R_1 = 1.6 \text{ cm}$ and $R_2 = 2.3 \text{ cm}$. The filter paper thickness $d_0 = 1.1 \text{ mm}$, and its porosity $\phi_{paper} = 0.22$ according to Meeten and Smeulders (1995).

Note that the adopted formulation in this study is different from the approach by Huisman and Van Kesteren (1998), which relies on Gibson's large strain theory, meaning the permeability of the mixture is dependent on consolidation as well. For dense slurries, small-strain assumption remains a good approximation, hence, Talmon (2026) theory is adopted.

The derived permeability can be further converted into hydraulic conductivity and subsequently resistance time with:

$$K = \frac{\rho g}{\mu} k \quad (2)$$

$$R_{CST} = \frac{H_s}{K \cdot (3600 \times 24)} \quad (3)$$

where K is the hydraulic conductivity (m/s), ρ is the density of water, g is gravitational acceleration (9.81 m/s^2), and μ is the dynamic viscosity of water ($\text{Pa}\cdot\text{s}$), R_{CST} is the resistance time (day) assuming a certain height of the soft solution layer (mixture layer) H_s (m).

Equations (1) and (2) can also be written as:

$$K = \frac{\rho g H}{P_{capi}} \frac{L_c}{\Delta t} \quad (4)$$

where L_c is the geometric dimensionless constant only associated with the experiment apparatus (Talmon et al., 2013):

$$L_c = \phi_{paper} \frac{d_0(R_1 + R_2)(R_2 - R_1)}{R^2} \quad (5)$$

3.3 Column tests with dynamic loadings

The primary purpose of the column test is to evaluate the permeability and physical stability of sediment mixtures under dynamic conditions that realistically simulate the hydraulic forces on the bottom of the channel due to inland shipping, moving beyond the static measurements of the CST test in a laboratory environment. While the CST test establishes a baseline, the Column test investigates how the soft solutions behave when subjected to dynamic shear stresses, specifically focusing on phenomena such as erosion of the soft solution layer, crack formation, and self-repairing capabilities. The test setup of the column tests is comparable to the setup of earlier tests performed in 2019 (Deltares 2019a). Most notable differences are that the vane operates differently with periodic rotation instead of continuous rotation and that a wider range of soft solutions is tested. The ARK conditions are used to define the parameters for the tests, but the outcomes are valuable in a more generic sense as well.

3.3.1 The setup of the column

The apparatus for conducting the column test consists of a transparent vertical column a diameter of 0.19 m (Figure 3-2). The entire column is made of two pieces, an upper piece and a bottom piece which can be joined together by screws. The design allows convenient preparation and cleaning of sediment materials before and after each test. The sediment profile

is constructed with a 0.3 m base layer of S90 sand, overlaid by a specific mixture layer designated for testing. A constant water level is maintained approximately 1.2 m above the base sand interface using a circulation system, where a pump feeds water from a reservoir to an inlet with a flow rate of 0.38 L/min while an overflow outlet regulates the designed water level. The hydraulic head is 1.5 m from the water level to the bottom of the column where pore water can flow out via a tube and the pore pressure is zero (equal to atmospheric pressure). The pressure head of 1.5 m is comparable to the pressure head of the ARK to the surrounding polders. Water permeating through the sediment layers passes through a 'Begemann' filter cloth at the base and drains through the bottom valve into a collection container positioned on an electronic scale, which records the cumulative mass of seepage water at a frequency of 1 Hz to quantify the permeability over time. To simulate the hydrodynamic shear stresses induced by shipping traffic, a programmable rotating vane is mounted within the water column roughly 5 cm above the surface of the mixture layer.

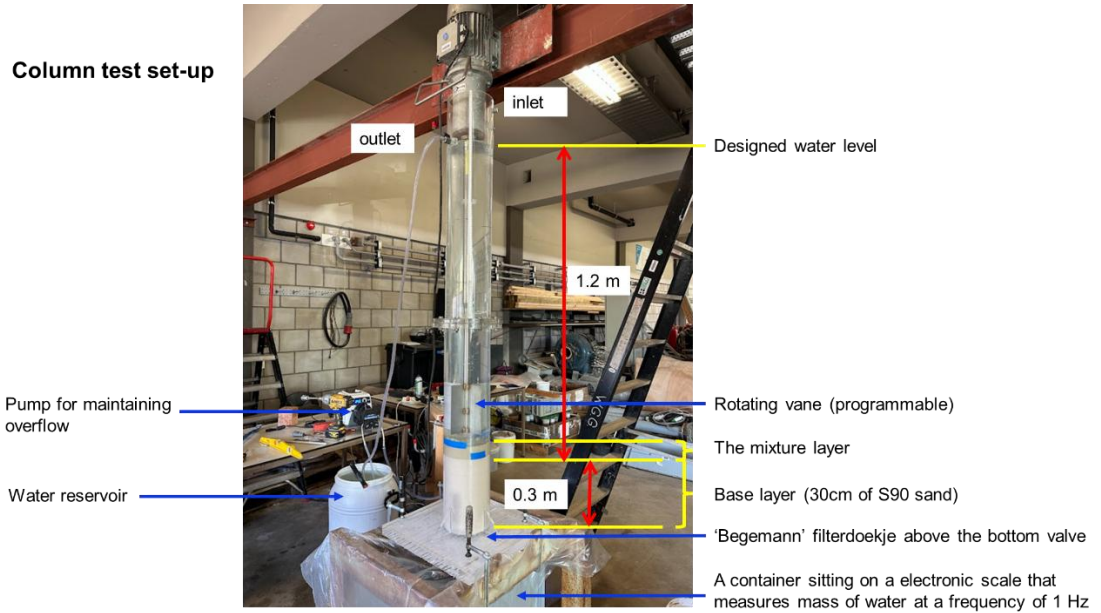


Figure 3-2. The setup of the apparatus for the column test

3.3.2 The protocol for vane operation

The vane used in the column test has four blades with an overall diameter of 17 cm and height of 20 cm. Because the gap between the vane blades and the wall of the column is only 1 cm, it is reasonable to assume that the fluid at the tip of the vane flows at a velocity equal to the vane rotating speed (Deltares, 2019a). This means that the flow velocity created by the rotation of the vane near the column wall can be approximated by:

$$U = \omega \cdot \frac{D_v}{2} = \pi D_v \cdot \frac{RPM}{60} \quad (6)$$

where U is the flow velocity at the tip of the vane (m/s), ω is the angular velocity at the vane tip (rad/s), D_v is the diameter of the vane (m), and RPM is the rotation of speed (s^{-1}). It is worth noting that towards the centre of the column, the flow velocity is substantially lower due to the decrease in the effective diameter of the vane.

For the specific type of the vane used in this study, its rotation speed (RPM) is a function of the applied voltage V :

$$RPM = 25 + V \cdot 150 \quad (7)$$

The formula above shows that the minimum attainable RPM is 25. To ensure the vane remains static for a certain designated period, a relay was integrated into the controller to disconnect the power supply whenever the input voltage is zero.

The protocol for the vane operation was carefully defined based on the field observations to ensure the column tests realistically impose dynamic shear stresses that are representative of the hydrodynamic conditions in the Amsterdam-Rhine Canal. A full test runs for approximately 17 hours, simulating an extended period with dynamic loadings. The vane is programmed to run in short, intermittent bursts to mimic frequent passages of ships.

The vane is activated every 15 minutes for a duration of 30 seconds. A passing ship event in ARK takes on average 30 seconds (Deltares 2025a). In the field campaign in ARK (Deltares 2025a) 10–15 ships per hour passed during the day in the canal and on average every 1.5 hours a ship generated a water level drop of >0.25 m resulting in a return current of 0.1-1.4 m/s. The 15-minute interval for vane operations in the column test is more frequent than the ships in ARK giving >0.25 m water level drop and less frequent than 10-15 ships per hour in ARK regardless of the water level drop.

The vane speeds are varied to represent different ship types and movements. The protocol uses a predefined distribution:

- 50% of actions at 0.6 m/s.
- 40% of actions at 1.2 m/s (slightly lower than the maximum ship-induced flow of 1.4 m/s measured in the 9-day field campaign in ARK (Deltares 2025a)).
- 10% of actions at 2.4 m/s (1.7x higher than the highest measured ship-induced flow velocity during the 9-day field campaign in ARK (Deltares 2025a), representing extreme events).

The operational protocol is structured into six distinct segments, each comprising 10 loading cycles: 5 cycles with 0.6 m/s; 4 cycles of 1.2 m/s; and 1 cycle of 2.4 m/s. The complete protocol is illustrated in Figure 3-3. At the start of the experiment and in the middle there is a one hour calm period without vane action to give the sediment time for settling.

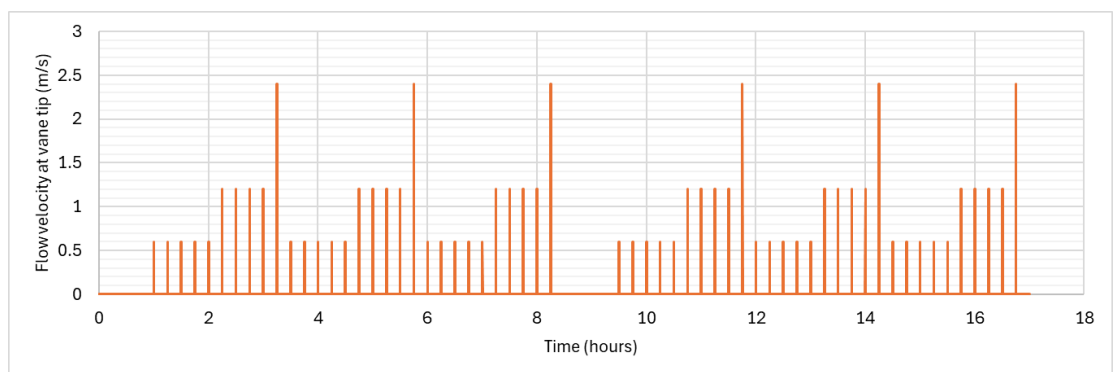


Figure 3-3. The protocol for the vane operation during column test

The shear stress at about 5 cm below the lowest part of the vane was determined at three different flow velocities in the previous study (Deltares, 2019a). It was assessed from the visual initiation of motion of sand particles with different sizes in the test setup. The derived bed shear stresses in Deltares (2019a) are used to calibrate a bed shear stress function to calculate the bed shear stresses of the vane speeds in present column tests (which differ from the 2019 vane speeds for which bed shear stress was derived). Bed shear stress can be calculated from the near bed flow velocity by the following formula:

$$\tau = \rho C_f U^2 \quad (8)$$

Where τ is the bed shear stress (Pa), ρ is the water density (kg/m³), C_f is a dimensionless drag coefficient and U is the flow velocity near the bed (m/s). For flow velocities at 100 cm from the bed Soulsby (1997) derived a range of empirical drag coefficients, e.g. $C_f = C_{100} = 0.003$ for mud/sand, $C_f = C_{100} = 0.0026$ for unrippled sand and $C_f = C_{100} = 0.0024$ for mud/sand/gravel or sand/gravel. The bed shear stress derived in the column tests of 2019 (Deltares 2019a) can be approximated by using $C_f = C_{100} = 0.0026$, which is a realistic value. Hence, we use this value to estimate the bed shear stresses of the vane action in the 2025 column tests. The final relationships between the vane rotation RPM, flow velocity at the vane tip and shear stresses can be seen in Table 3-1.

Table 3-1. The vane rotation speed, flow velocity at the vane tip and the corresponding shear stress at 5 cm below the vane in the column tests.

RPM	U (m/s)	Shear stress derived in 2019 column test (Deltares 2019a) (Pa)	Calculated shear stress with Eq. 6 by using $C_f = 0.0026$ (Pa)
0	0.0		0
72	0.6	~0.7	0.9
84	0.7	~1.2	1.3
144	1.2	~4.2	3.7
288	2.4		15

The vane tip speeds of 0.6, 1.2 and 2.4 m/s in the protocol correspond to a calculated shear stress of respectively 0.9, 3.7 and 15 Pa. These shear stresses in the column test are similar in magnitude to the measured shear stresses of ship passages in ARK. The field measurements show a maximum shear stress of 17 Pa with the majority of the ship passages leading to a shear stress < 1 Pa and the majority of ships going over the monitoring frame giving 1-4 Pa (Deltares 2025a).

The similarity of the vane velocity magnitude and shear stresses with the measured field conditions in ARK ensures that the damage and material response measured in the column are relevant to real-world sealing performance. The highest vane speed of 2.4 m/s in the column tests is 1.7x higher than the highest measured ship-induced flow velocity, but the corresponding bed shear stress from the vane of approximately 15 Pa corresponds to the highest measured shear stress of 17 Pa in the 9-day field campaign in ARK (Deltares 2025a). Given the limited measurement period of 9 days in the field campaign it is possible that incidentally higher ship-induced flow speeds occur in the ARK. The occurrence of the high shear stresses in the vane protocol is more frequent than in the field measurements. Hence, the applied vane protocol is considered to be representative, but on the conservative side for ARK conditions.

The repeated, cyclical loading sequence forces the sediment mixture to respond dynamically: erosion and resuspension may occur under high velocity, leading to temporary spikes in permeability, and the material's ability to remix and self-repair during the subsequent rest period is then evaluated by monitoring the long-term stabilization of the leakage rate. ZBM is prone for crack formation when the bentonite consolidates and resuspension of fines helps to seal those cracks, which is a self-healing property of ZBM (Deltares 2019b, 2020, Van Heteren 2020, Witteman 2024). The vane action is also suitable to investigate this self-healing behaviour of ZBM.

3.3.3 The preparation of the test

During the preparation of each test within the project, a few lessons were learned after trial and error:

- The base sand layer acts as a proxy for the canal bottom and must remain saturated and compacted throughout the testing program. To achieve this, the protocol involves saturating the base layer and subsequently forcing compaction via mechanical vibration while the bottom valve is open.
- The soft solution layer (mixture layer) should be placed on top of the base layer with the column's bottom valve open. Opening the valve creates negative (excess) pore pressure at the interface which, added to the static water head, provides the required total hydraulic pressure. This process also forces the two layers to integrate at their interface, forming an immediate sealing layer.
- Following the placement of the mixture layer, water must be introduced gently to prevent surface disturbance. This precaution ensures the layer remains in a homogenous and undamaged condition prior to testing.
- The electric scale Sartorius CP34000 was used in the study. This specific model has built-in digital filter and drift compensation function (auto-zero tracking). This means that when it starts with zero and water drops fall slowly, the scale may ignore slow drip accumulation. It is recommended to tare the empty bucket, then activate the weighing system by adding a small amount of water quickly (~4-5 g), or simply disable the auto-zero tracking function in the scale. Unfortunately, the auto-zero tracking function has impacted the outcomes of the earlier moments in some tests. For the tests considered, this will be mentioned.

3.3.4 Interpretation of the results

The column test measures the mass of water leaking through the mixture layer and the based sand layer under the dynamic loadings. The performance of each soft solution can be quantified by calculating the resistance time from the measurements (Deltares, 2019a).

$$R_{column} = \frac{dp}{q_f} \cdot \frac{1}{24 \times 3600} \quad (9)$$

$$q_f = \frac{(m_{t+\Delta t} - m_t)}{\rho A \Delta t} \quad (10)$$

where R_{column} is the resistance time (day), dp is the water level difference (m) between the canal and the surrounding groundwater (in our case the total hydraulic head), q_f is the filtration velocity (m/s), Δt is the time interval (s) between the measured water mass $m_{t+\Delta t}$ and m_t (kg) at time $t + \Delta t$ and t respectively, ρ is the density of water (kg/m^3), and A is the cross-section area of the column (m^2). Seepage through the canal bottom (or column test bed) scales with one divided by hydraulic resistance time. Hence, an increase of R from 1 day to 10 days will reduce the seepage with a factor 10.

The hydraulic conductivity K can be computed according to:

$$K = \frac{q_f}{I} = \frac{q_f \cdot h_e}{dp} \quad (11)$$

where I is the pressure gradient (-), which is the total hydraulic pressure dp (m) divided by the thickness of the effective layer h_e (m) functioning as the filter cake.

4 Results

4.1 Results CST tests

4.1.1 Reference case

The primary objective of the Capillary Suction Time (CST) testing phase was to characterize the permeability of various sediment mixtures and establish specific "recipes" for the subsequent column tests. To ensure comparability, a reference standard was established using a Premixed Sand-Bentonite (ZBM supplied by Van Heteren) material. The baseline properties of the Premixed Sand-Bentonite were measured as follows:

- Mixture density: 1.2922 g/cm³
- Water content: 178.2 %
- Average CST time: 1832.5 s
- Hydraulic conductivity: 1.0×10⁻⁸ m/s

The hydraulic conductivity is derived from the measured CST time according to eq. (1) by defining the filter paper porosity $\phi_{paper} = 0.22$. This value is adopted from Meeten and Smeulders (1995), who conducted a comprehensive investigation into the properties of this specific filter paper and other relevant CST test parameters. Notably, the hydraulic conductivity of the ZBM determined in this study is consistent with the range observed in geotechnical tests from the previous study (Deltares, 2020).

Based on this reference material, two target resistance values were defined to guide the formulation of other mixtures. These targets correspond to the theoretical hydraulic resistance provided by specific layer thicknesses of the reference ZBM:

- **Low Resistance Target:** Equivalent to a 4 cm layer of Premixed ZBM leading to calibrated CST resistance of ~ 44 days.
- **High Resistance Target:** Equivalent to an 8 cm layer of Premixed ZBM leading to calibrated CST resistance of ~ 88 days.

In this manner the column tests for all homogeneous mixtures are conducted with a start hydraulic resistance comparable to either 4 cm Premixed ZBM or 8 cm Premixed ZBM. Both target hydraulic resistance values will result in a very big reduction of seepage compared to a situation with a sandy canal bottom. As a reference, the target hydraulic resistance of 44 and 88 days would require a sand layer of approximately 400 m, respectively 800 m.

Next two sections will discuss the CST results of the different soft solutions. At the end a summarizing table is provided with the recipe of each soft solution and the resulting hydraulic resistance found in the CST tests.

4.1.2 Results of sand-material mixtures

For the alternative materials (OCMA bentonite, S1 clay, dredged mud, and granulite), mixtures were prepared with sand to act as potential soft solutions for sealing the canal bottom. To approximate the status of a compacted sediment layer placed at the bottom of the canal and maintain consistency throughout the tests, the porosity for all prepared mixtures was controlled at approximately 0.5. Half the mixture volume consists of solids and the other half of the volume consists of pores filled with pore water. This porosity is considered representative for a porosity of recently placed or stirred soil and is slightly lower than the in-situ porosity of a non-stirred sand bed which has a typical porosity around 0.4.

For each type of sand-material mixture, CST tests were performed at varying recipes (varying volumetric ratio between sand and the alternative material) to establish a better understanding regarding the resistance time and the mixture composition. During the tests, 2-3 replicates were usually performed and the average CST was reported. From the derived curves, two specific recipes were selected to approximate the low and high resistance targets defined above.

Table 4-1 presents the material dry densities used to formulate the mixtures. These parameters were derived via pycnometer measurements following a three-step procedure: preparing water dilutions, assessing the mixture density, and measuring water content after drying the samples in an oven overnight. The specific solids density can be computed by the following formula:

$$C_s = \rho_m \cdot \frac{1}{1 + w} \quad (12)$$

$$V_s = 1 - V_w = 1 - \frac{\rho_m}{\rho_w} \cdot \frac{w}{1 + w} \quad (13)$$

$$\rho_s = \frac{C_s}{V_s} = \frac{\rho_m \cdot \rho_w}{\rho_w(1 + w) - w \cdot \rho_m} \quad (14)$$

where ρ_s is the specific solids density (g/cm³), ρ_m is the mixture density of the dilution (g/cm³), ρ_w is the density of water (1.0 g/cm³), C_s is the mass concentration of solids (g/cm³), V_s is the volumetric concentration of solids (cm³/cm³), w is the water content (-), $w = m_w/m_s$ and $1 + w = (m_w + m_s)/m_s$, m_s is mass of solids and m_w is mass of water.

Table 4-1. The measured solids density of the materials.

Sediment type	Solids density (g/cm ³)
OCMA Bentonite	2.300
Granulite	2.600
S1 clay	2.423
Dredged mud	2.490
S90 Sand	2.650

A selection of the tested sand-material mixtures data is shown in Figure 4-2 - Figure 4-5. For each type of material, a specific volume of sand was added to maintain a constant mixture porosity of 0.5. By systematically varying the sand-to-material composition, the relationship between resistance time (assuming a layer thickness of 40 cm) and mass ratio of sand fraction to material fraction, hereafter referred to as the sand-fines ratio (SFR), was established. This relationship is based on the observation that, for sand-material mixtures with constant porosity, permeability is primarily controlled by the SFR, which reflects the relative abundance of fine sediment within the mixture. These trends were subsequently quantified by fitting a power law regression to the measured data. The red circles within these figures indicate the specific recipes that match the high and low targeted permeability values, hence were chosen for the column tests. Detailed information regarding each recipe can be found in the Appendix.

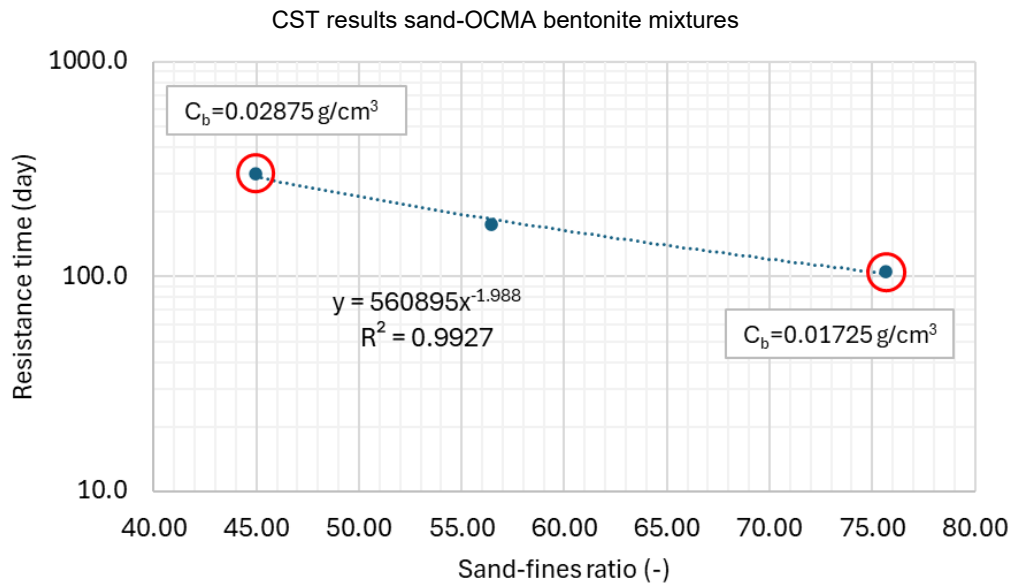


Figure 4-2. The derived resistance time (assuming a 40 cm thick mixture layer) and the fitted power law as a function of the sand-fines ratio of the sand-OCMA bentonite mixtures. C_b is the mass concentration of bentonite of the selected recipe.

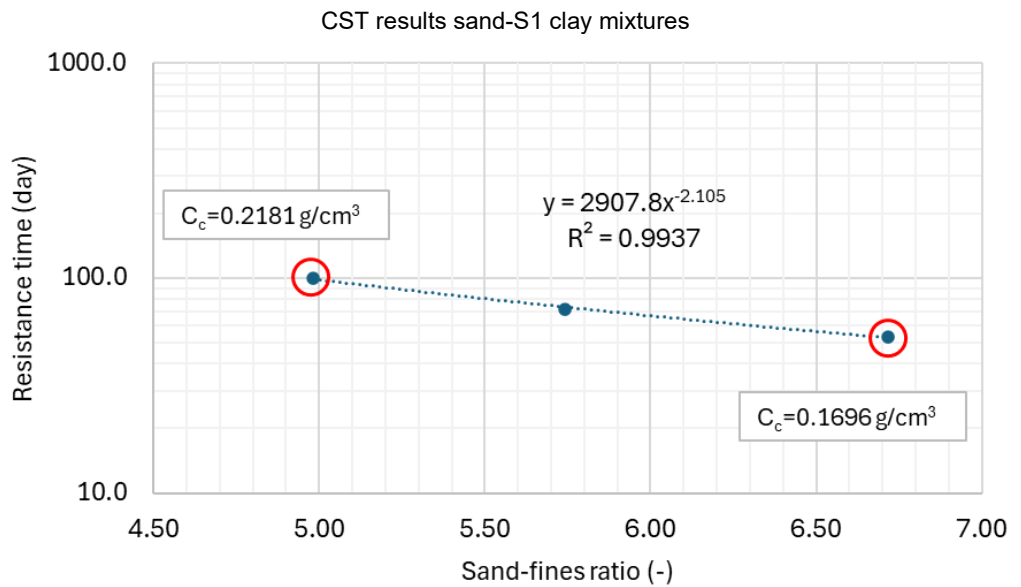


Figure 4-3. The derived resistance time (assuming a 40 cm thick mixture layer) and the fitted power law as a function of the sand-fines ratio of the sand-S1 clay mixtures. C_c is the mass concentration of clay of the selected recipe.

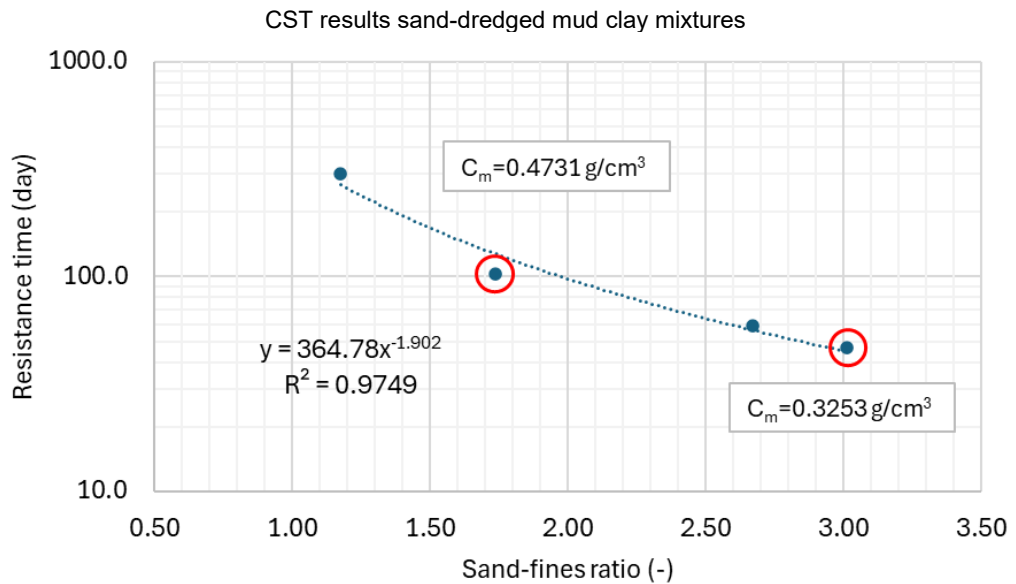


Figure 4-4. The derived resistance time (assuming a 40 cm thick mixture layer) and the fitted power law as a function of the sand-fines ratio of the sand-dredged mud mixtures. C_m is the mass concentration of dredged mud of the selected recipe.

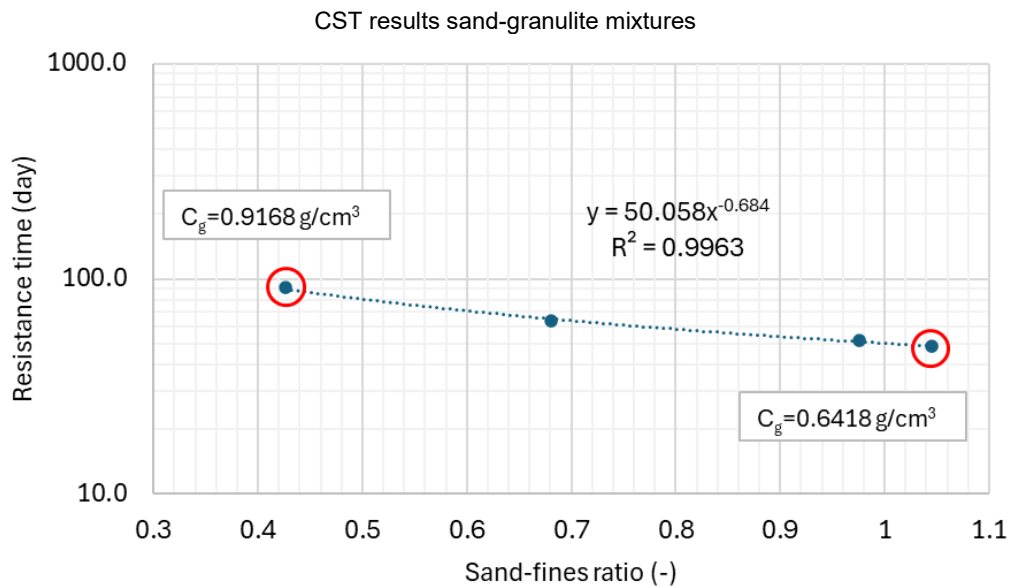


Figure 4-5. The derived resistance time (assuming a 40 cm thick mixture layer) and the fitted power law as a function of the sand-fines ratio of the sand-granulite mixtures. C_g is the mass concentration of granulite of the selected recipe.

Across all four material types, there is a consistent negative power-law relationship between mixture density and resistance time for a 40 cm thick mixture layer. Since the porosity is fixed at 0.5, an increase in mixture density typically correlates with a higher proportion of sand (which is denser and more permeable) and a lower proportion of the fine sealing material. Therefore, as mixture density increases, the hydraulic conductivity drops sharply.

It is worth noting that for the Sand-OCMA Bentonite mixture, the minimum achievable resistance time in the CST tests is constrained by the bentonite volume fraction.

In the low concentration case (below the 0.75% threshold), the mixture segregates immediately after mixing because the bentonite suspension is too dilute. Consequently, we could not achieve the lower target resistance times seen with other materials for a layer thickness of 40 cm, and the lowest achievable resistance time here is comparable to the High Resistance Target (~ 100 days). To approximate ZBM performance, the high concentration case was established by increasing the bentonite volume fraction to 1.25%, which resulted in a threefold increase in resistance time compared to the low concentration case. This demonstrates the high sensitivity of the resistance time to the bentonite fraction.

The most significant trend observed from the tested sand-material mixtures is the vast difference in efficiency (sealing capability per unit mass) between the materials. To achieve similar target resistance times (roughly 40-50 days for low concentration and 80-100 days for high concentration, assuming a 40 cm thick mixture layer), the required mass concentrations vary by orders of magnitude:

- OCMA bentonite: Most efficient, requiring only $\sim 0.02 - 0.03 \text{ g/cm}^3 = \text{t/m}^3$.
- S1 clay: Moderately efficient, requiring $\sim 0.17 - 0.22 \text{ g/cm}^3 = \text{t/m}^3$.
- Dredged mud: Less efficient, requiring $\sim 0.32 - 0.47 \text{ g/cm}^3 = \text{t/m}^3$.
- Granulite: Least efficient, requiring $\sim 0.64 - 0.92 \text{ g/cm}^3 = \text{t/m}^3$.

As can be seen, the sand-OCMA bentonite demonstrates the highest efficiency, achieving target resistance times with very low mass concentrations. In contrast, the sand-S1 clay requires approximately 10 times that mass to achieve comparable performance. The efficiency drops further for the sand-dredged mud and is lowest for the sand-granulite mixtures, which require nearly 30 to 50 times more granulite than the concentration of bentonite, to generate equivalent permeability. For pure granulite the CST results would be very different, but as explained in Section 2.1, pure granulite is not included in the 2025 test series because in the 2019 tests (Deltares 2019a) water was leaking at the interface granulite-plexiglass of the column tests which influenced the results significantly.

4.1.3 Results of pure clay and pure dredged mud

In addition to investigating various sand-material mixtures, another key objective in this study is to assess the permeability of clay and natural mud in their pure states without a sand skeleton. For each type of material, several dilutions were created and subsequently tested for their permeability using CST tests. The derived resistant time is plotted against excess density compared to water ($\rho_m - \rho_w$). For these pure mixtures, excess density serves as a direct proxy for solids concentration. The resulting power-law relationship aligns with fractal dimension theory, where the fitted exponent quantifies the compactness and structural complexity of the particle matrix formed within the mixture (a higher value implies a more compact and denser structure).

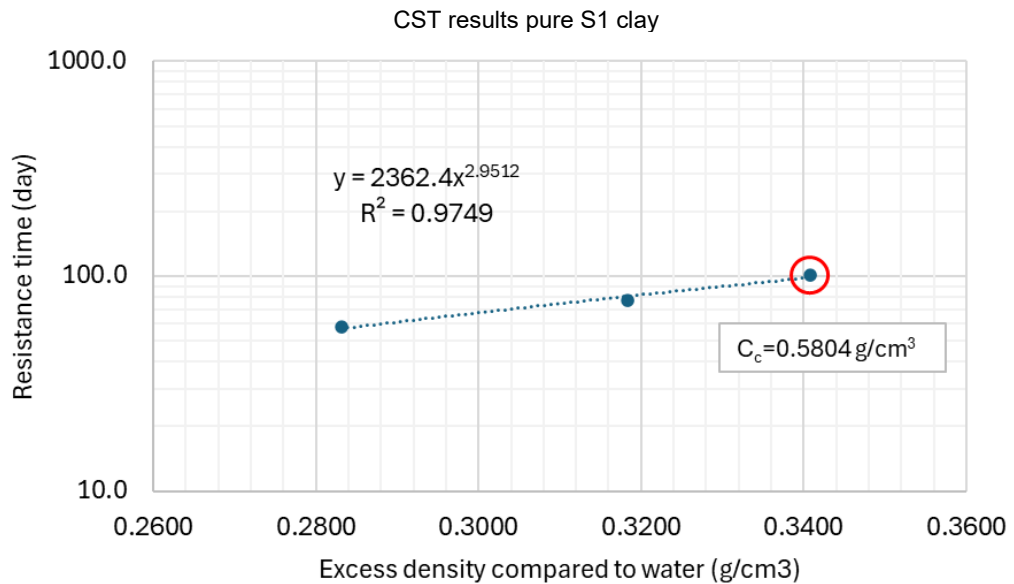


Figure 4-6. The derived resistance time (assuming a 40 cm thick layer) and the fitted power law as a function of the excess density of pure S1 clay mixtures. C_c is the mass concentration of clay of the selected recipe.

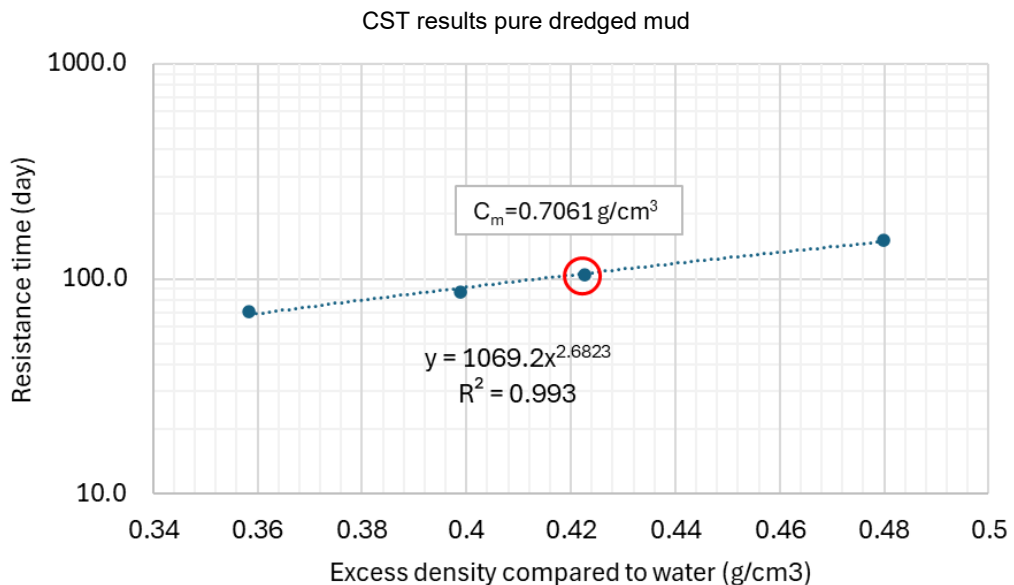


Figure 4-7. The derived resistance time (assuming a 40 cm thick layer) and the fitted power law as a function of the excess density of pure dredged mud. C_m is the mass concentration of dredged mud of the selected recipe.

Again, the resistance time is computed from the measured permeability (or hydraulic conductivity), assuming a 40 cm thick layer of pure material. In these "pure" configurations, there is a strong positive power-law correlation between resistance time and excess density. As illustrated in Figure 4-6 for pure S1 clay and Figure 4-7 for pure dredged mud, an increase in mixture density corresponds to a significant rise in resistance time. This trend indicates that for pure slurries, higher density reflects a higher solids content (and lower water content), which creates a tighter matrix and enhances the sealing capacity. The red circles identify the specific target recipes chosen for further column testing: the pure S1 clay recipe was selected at a clay

mass concentration of 0.58 t/m³, while the pure dredged mud recipe required a higher mass concentration of 0.71 t/m³ to achieve a similar resistance profile near the 100-day mark.

In contrast, in the sand-material mixtures, the total solids concentration remains constant due to the fixed porosity. Consequently, the concentration of the cohesive fraction (expressed via the sand-fines ratio) becomes the primary influencing factor of permeability and the resulting resistance time. Hence, the established power laws are also different.

4.1.4 Overview of the tested recipes

The results of the tested recipes discussed above are summarized in **Error! Reference source not found.**

Table 4-1 CST results of the tested recipes

Tested recipe	Volumetric conc. of sand (-)	Volumetric conc. of material (-)	Mass conc. of sand (g/cm ³)	Mass conc. of material (g/cm ³)	Sand-fines ratio	Resistance time of a 40 cm layer (day) based on CST results
Sand-OCMA bentonite (high)	0.4875	0.0125	1.2919	0.0288	44.9	300
Sand-OCMA bentonite (low)	0.4925	0.0075	1.3051	0.0173	75.4	106
Sand-S1 clay (high)	0.4100	0.0900	1.0865	0.2181	5.0	101
Sand-S1 clay (low)	0.4300	0.0700	1.1395	0.1696	6.7	54
Sand-dredged mud (high)	0.3100	0.1900	0.8215	0.4731	1.7	104
Sand-dredged mud (low)	0.3694	0.1306	0.9788	0.3253	3.0	47
Sand-granulite (high)	0.1474	0.3526	0.3905	0.9168	0.4	91
Sand-granulite (low)	0.2532	0.2468	0.6709	0.6418	1.0	48
Pure S1 clay	N/A	0.2400	N/A	0.5804	N/A	102
Pure dredged mud	N/A	0.2836	N/A	0.7061	N/A	105

4.2 Results column tests with vane

As described in §3.3, each column test was carried out over a period of 17 hours, in which the dynamic loading was introduced by operating a vane according to a predefined protocol. During the test, the cumulative mass of seepage water was recorded over time. Later, the measured data was processed and translated into filtration velocity and resistance for interpretation. The details regarding the data processing is described in Appendix 7A.1.

4.2.1 ZBM test results (solutions applied in the Twentekanaal)

Figure 4-8 and Figure 4-9 show the column test setup for the Premixed Sand-Bentonite material (ZBM by Van Heteren) at both the High Resistance Target (8 cm layer) and the Low Resistance Target (4 cm layer). These two reference tests form a stable baseline against which the performance of all other materials (clay, mud, granulite) and their failure modes (erosion, cracking) can be compared. Additionally, these two tests provide insight in the response of ZBM to the periodic shear from the vane. The results of the tests can be found in Figure 4-10 and Figure 4-11.



Figure 4-8. The initial setup of the test (based sand layer plus ZBM layer of 8 cm) on the left and the final state of the layers after the test on the right.



Figure 4-9. The initial setup of the test (based sand layer plus ZBM layer of 4 cm) on the left and the final state of the layers after the test on the right.

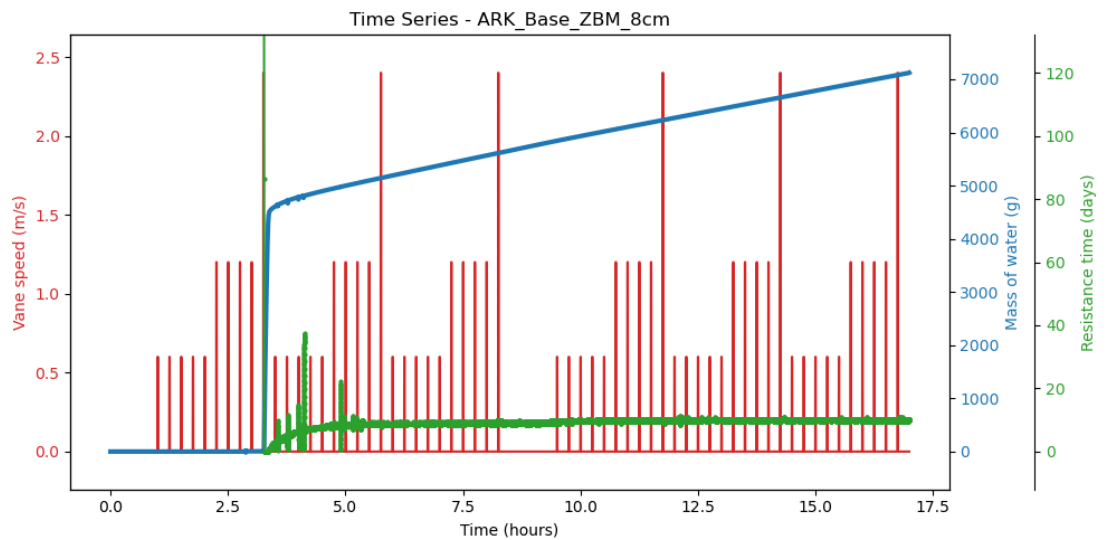


Figure 4-10. The measured mass of water during the test, the speed of vane rotation and the derived resistance time (base sand layer plus a ZBM layer of 8 cm).

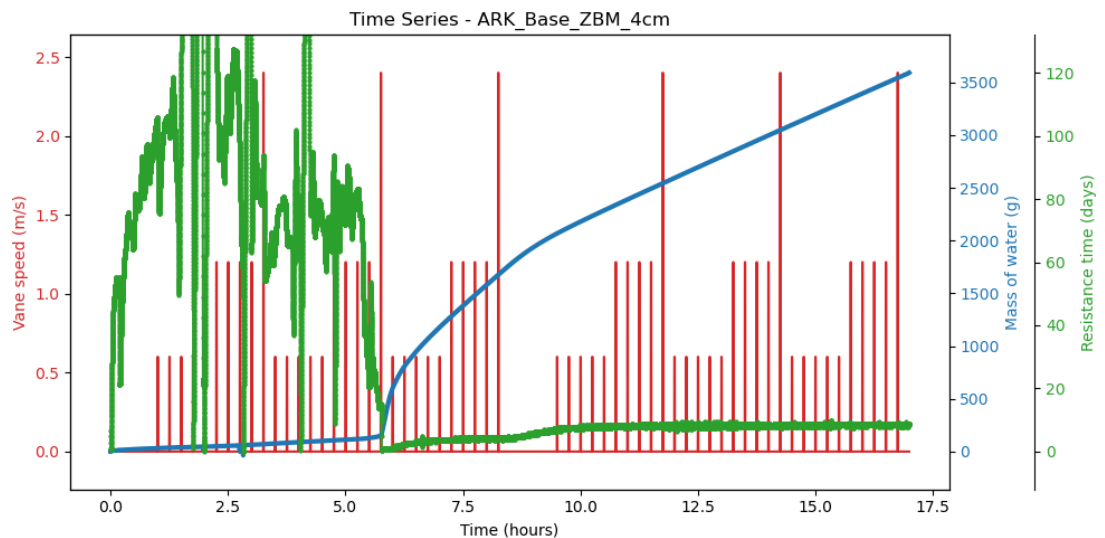


Figure 4-11. The measured mass of water during the test, the speed of vane rotation and the derived resistance time (base sand layer plus a ZBM layer of 4 cm).

The reference tests conducted on Premixed Sand-Bentonite (ZBM) layers of 8 cm and 4 cm revealed a distinct hydro-mechanical response characterized by bulk erosion followed by interfacial stabilization. Visual inspection of the final column states indicates that the majority of the initial ZBM overburden was eroded by the hydrodynamic shear, resulting in high turbidity due to suspended bentonite particles. This physical degradation is verified by the time-series data, which recorded critical failure events, occurring at approximately 3.5 hours for the 8 cm layer and 5.5 hours for the 4 cm layer, marked by a sharp vertical surge in water leakage and a collapse of resistance time to near-zero values. Since crack formation is typically a gradual process associated with low-shear conditions, the failure observed during the high-shear vane action was likely caused by insufficient internal shear strength within the ZBM layer. The combination of erosion and high shear stress appears to have degraded the layer's integrity, leading to structural failure.

However, a recovery phase started immediately after these failure events once the highest velocity cycle (2.4 m/s) ended. The transition to lower velocity cycles and short resting intervals facilitated the material's re-stabilization under the hydraulic pressure. Despite the continued application of dynamic loading and the loss of the bulk material, the resistance in both tests gradually rebounded and stabilized, reaching approximately 10 days for the 8 cm case and 8 days for the 4 cm case by the end of the test. These end stage resistance values in the tests remained constant during the last 30 cycles of vane action, including 3 high velocity 2.4 m/s vane actions. During the start of the test the high velocity 2.4 m/s vane action destroys the ZBM layer, but the ZBM layer that after this initial failure subsequently builds up during the test is not destroyed by 2.4 m/s vane actions anymore. This resilience confirms the hypothesis that while the bulk layer is susceptible to erosion under high shear, a thin, robust functional layer forms at the base layer-mixture interface. In this zone, the residual sand and bentonite remix and consolidate, providing a durable sealing effect that persists even after the primary layer is compromised.

Furthermore, the bentonite particles suspended in the water column likely function as a material reservoir for self-healing (Deltares 2019b, Van Heteren 2020). Under the influence of the hydraulic gradient, these fine particles are drawn into the voids in between sand skeleton of the base sand layer at the interface, effectively resealing the matrix whenever preferential flow paths emerge. The abundance of suspended bentonite in the water column ensures an ample

supply of material for self-healing, effectively decoupling the final sealing capacity from the initial layer thickness. The end resistance found in this setup of the 8 cm ZBM layer is only 20% more than that of the 4 cm ZBM layer, but it is expected that the 8 cm ZBM layer will have more self-healing capacity as there is more buffer of suspended bentonite.

In the 2019 column tests (Deltares 2019a) only one test with ZBM applied the vane, which was a 5 cm ZBM test, see Figure 4-12 for a repetition of the 2019 result of this test. In 2019 the 5 cm ZBM column test started with 19 hours without vane, followed by 1 hour with a stepwise slowly increasing vane action from 0.2 to 5.8 m/s tip speed. In this initial 19 hours without vane action the hydraulic resistance slowly increased to a value of ~55 days. After the initial vane action of 0.2 m/s the resistance dropped to ~15 days, probably due to the handling and stirring influence of applying the vane and not from the 0.2 m/s tip speed. Then the vane speed is slowly increasing in one hour time and up to a vane speed of 3.6 m/s after ~50 minutes, the resistance has increased again to ~45 days. For vane tip speeds of 4.8 and 5.8 m/s the resistance starts to decrease to ~20 days. Hence, when comparing the 2025 ZBM test and the 2019 ZBM test there is a remarkable different influence of the vane. In 2019 the vane did no harm to the resistance of the ZBM up to speeds of 3.6 m/s and in the 2025 test the vane peak speed of 2.4 m/s is already able to destroy the initial ZBM layer, but not the final ZBM layer. We hypothesize that the time that a ZBM is given to settle and build up is responsible for this difference. In the 2019 test the ZBM layer was given 19 hours of rest and in the 2025 test there is only 1 hour of complete rest and the first high vane speed action of 2.4 m/s occurs within 3 hours. Another difference between the 2019 vane action and the 2025 vane action is that in 2019 the vane slowly increases its speed without pauses and in 2019 the vane has a more realistic protocol with vane action for 30 seconds followed by 14.5 minutes of rest. Our expectation is that the difference in vane protocol is less important than the difference in initial resting time for the ZBM layer. It is advised to investigate the influence of vane action in relation to resting time for ZBM in more detail in follow up column tests as this appears to be an important factor for the functioning of ZBM and is also an important consideration for the necessity of a temporary pause in shipping during placement of ZBM in the ARK.

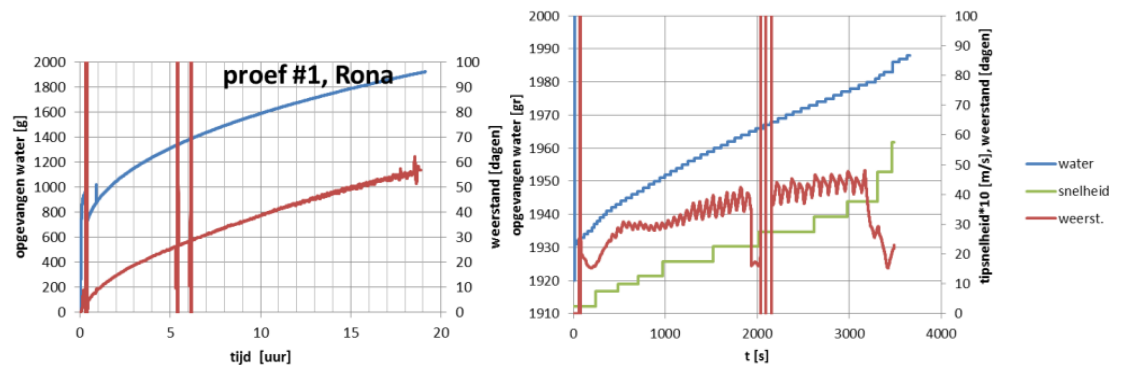


Figure 4-12 Result 2019 column test ZBM 8 cm layer (Deltares 2019a), left results of first 19 hours without vane and right results of last hour with vane action.

4.2.2 Sand – OCMA bentonite test results (soft solution with 40 cm layer)

The dynamic performance of Sand-OCMA bentonite mixtures was evaluated using 40 cm layers prepared at both high ($C_b \approx 0.029 \text{ g/cm}^3$) and low ($C_b \approx 0.017 \text{ g/cm}^3$) concentrations. Visual documentation of the experimental progression (Figure 4-13 and Figure 4-14) confirms the damage and recovery mechanism identified in the reference ZBM tests: the initially homogenous mixture layers proved structurally unstable under dynamic shear, especially with the highest velocity at 2.4 m/s. The mixture layer was undergoing significant erosion and segregation. The final states in both tests exhibit a turbid water column filled with suspended bentonite fines, while the coarser sand fraction has settled.



Figure 4-13. The initial setup of the test (based sand layer plus a sand-OCMA bentonite mixture layer of 40 cm - high bentonite concentration) on the left and the final state of the layers after the test on the right.



Figure 4-14. The initial setup of the test (based sand layer plus a sand-OCMA bentonite mixture layer of 40 cm - low bentonite concentration) on the left and the final state of the layers after the test on the right.

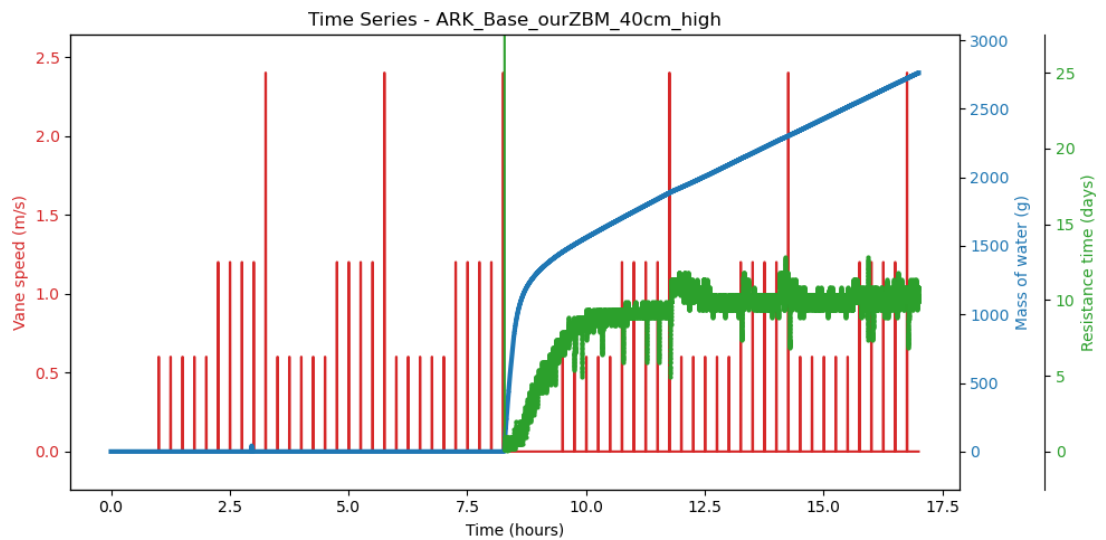


Figure 4-15. The measured mass of water during the test, the speed of vane rotation and the derived resistance time (base sand layer plus a sand-OCMA bentonite mixture layer of 40 cm with high bentonite concentration).

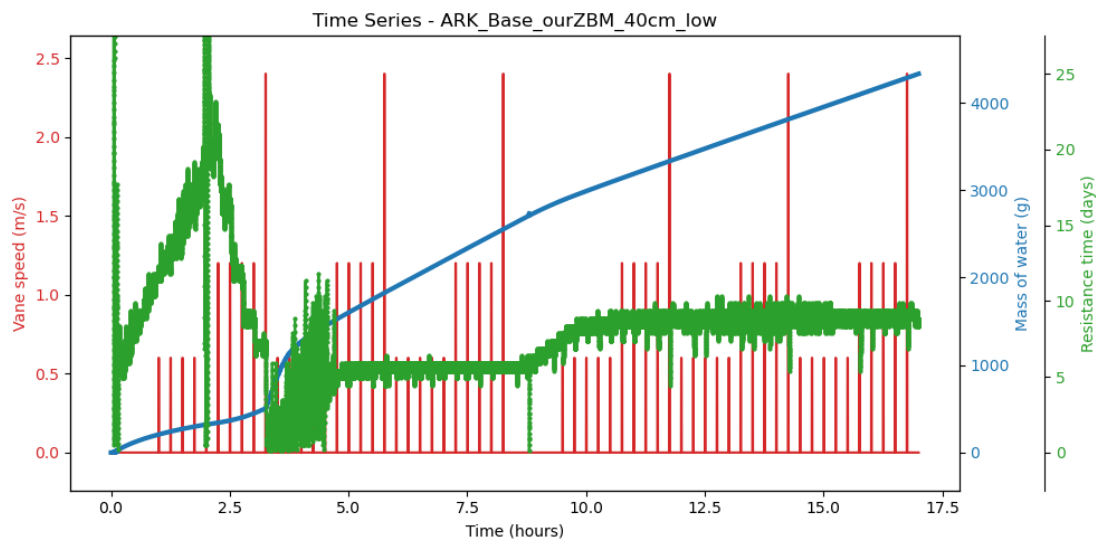


Figure 4-16. The measured mass of water during the test, the speed of vane rotation and the derived resistance time (base sand layer plus a sand-OCMA bentonite mixture layer of 40 cm with low bentonite concentration).

However, the quantitative time-series data (Figure 4-15 and Figure 4-16) reveals that this physical degradation did not compromise the sealing function. Both mixtures established stable hydraulic resistance profiles by the end of the loading cycle, with the high-concentration specimen achieving a resistance of approximately 10 days and the low-concentration specimen stabilizing near 9 days. These results support the conclusion that the initial layer thickness and configuration are less critical than the dynamic remixing process. Under the influence of the hydraulic gradient, a thin but highly effective functional layer forms and consolidates at the interface, while the abundance of suspended bentonite acts as a continuously available material reservoir to heal preferential flow paths, thereby ensuring long-term performance stability.

The testing of sand-bentonite mixtures provided useful insights into the structural evolution of the mixture layer, particularly in the beginning phase, within the low-concentration dataset. While data for the high-concentration case was masked during the first 8 hours due to the scale's drift compensation threshold, which may imply that early leakage rates were too low to register and that the layer remained crack-free, both scenarios likely followed a similar, tri-phasic response pattern. Initially, under the low-velocity regime (0.6 m/s), the mixtures demonstrated increasing resistance, a behaviour possibly attributed to self-weight consolidation. However, the transition to higher velocity cycles resulted in a decline in resistance, signalling the onset of erosion and damage to the effective layer. The extreme velocity cycles (2.4 m/s) proved to be the most destructive, consistently driving the strongest reductions in sealing capacity. After the erosion of the initial sand bentonite layer, subsequent deposition results in a more stable bed configuration with restored sealing performance, which is able to withstand the last 30 cycles of vane action, including 3 high velocity 2.4 m/s vane actions.

It is interesting to point out that the sand-OCMA bentonite mixtures with high and low bentonite concentration and 4 and 8 cm ZBM all four reached a comparable resistance time in the end of the test of 8-10 days, suggesting that an effective layer was formed with comparable characteristics in all four cases after the damage to the original mixture layer.

4.2.3 Sand – S1 clay test results (soft solution with 40 cm layer)

The experimental configuration for the Sand-S1 Clay mixtures involved a 40 cm overburden layer prepared at high ($C_c \approx 0.218 \text{ g/cm}^3$) and low ($C_c \approx 0.170 \text{ g/cm}^3$) concentrations, placed on top the standard compacted sand base layer (see Figure 4-17 and Figure 4-18). Visual inspection of the final states reveals a structural evolution analogous to the premixed ZBM and sand-OCMA bentonite cases: the dynamic hydraulic loading caused extensive erosion of the initial bulk mixture. The fine clay fraction was largely stripped from the sand skeleton and remained suspended in the water column, resulting in high turbidity. Consequently, the sealing function relied mostly on the formation of a remixed, consolidated interface layer between the eroded sediment and the base sand. Unlike the highly cohesive bentonite residues, the visual interface in the S1 clay tests appears slightly less distinct, partially due to the similarity in the colours of clay and sand particles. The column after the tests showed a layered structure: from top to bottom, a clay suspension in the upper column (dilute near the surface and more concentrated towards bottom), a mixed layer of clay and sand, with the sand fraction increasing downwards, an remaining effective layer and the beneath sand base layer. The measured resistance time suggests a potentially more fragile restructuring process.



Figure 4-17. The initial setup of the test (based sand layer plus a sand-S1 clay mixture layer of 40 cm - high clay concentration) on the left and the final state of the layers after the test on the right.



Figure 4-18. The initial setup of the test (based sand layer plus a sand-S1 clay mixture layer of 40 cm - low clay concentration) on the left and the final state of the layers after the test on the right.

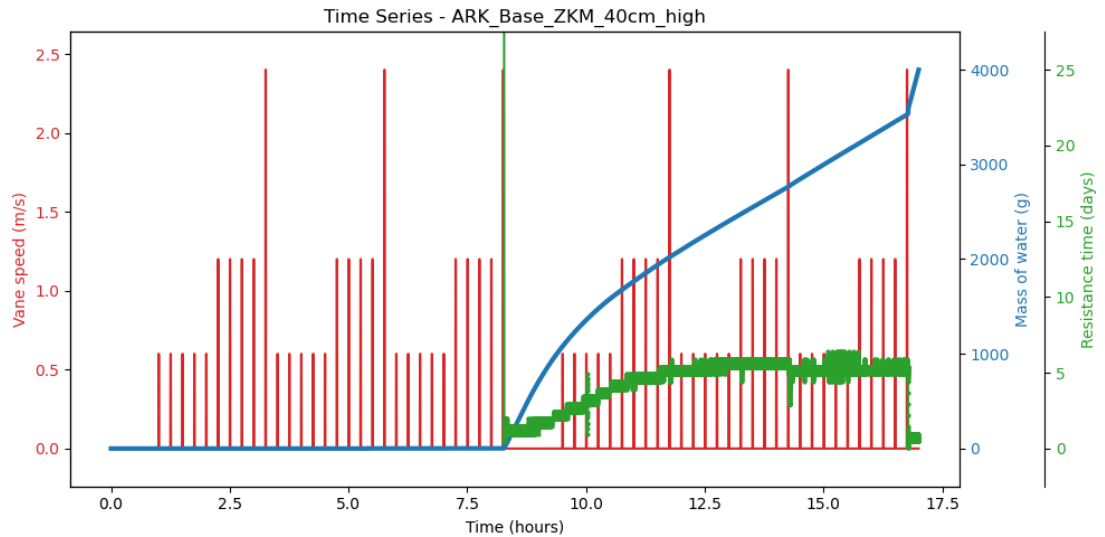


Figure 4-19. The measured mass of water during the test, the speed of vane rotation and the derived resistance time (base sand layer plus a sand-S1 clay mixture layer of 40 cm with high clay concentration).

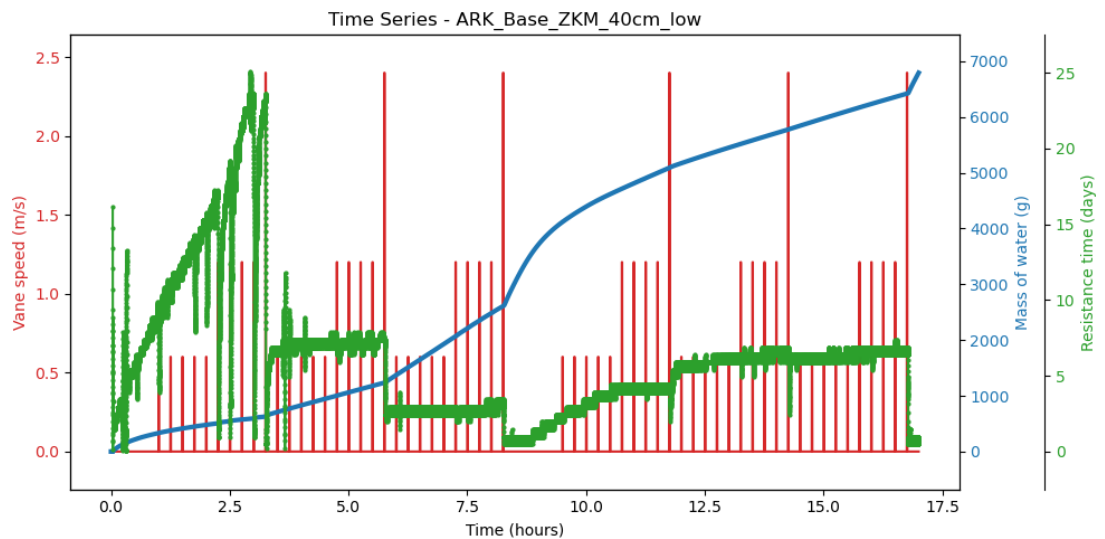


Figure 4-20. The measured mass of water during the test, the speed of vane rotation and the derived resistance time (base sand layer plus a sand-S1 clay mixture layer of 40 cm with low clay concentration).

The quantitative results presented in Figure 4-19 and Figure 4-20 confirm that the Sand-S1 Clay mixtures initially mimic the behaviour of the reference bentonite cases, displaying a cycle of consolidation, shear-induced failure, and partial recovery. In the low-concentration case, the mixture exhibited a distinct consolidation phase (0–3 hours) where resistance increased, followed by a sharp decline due to erosion as vane speeds increased. Both concentration cases suffered critical failure events near the peak velocity cycle (2.4 m/s), followed by a "self-repairing" phase where resistance recovered to approximately 5–7 days. It is worth noting that water leakage remaining zero in the first 8.5 hours in the high clay concentration test was likely due to the drift compensation of the electric scale, indicating a slow water leakage.

However, a critical deviation from the stable bentonite behaviour is observed in the final hours of testing the sand-S1 clay mixtures. In both high and low concentration cases, the resistance

time begins to decrease sharply near the end of the last cycle (around hour 16–17). This indicates that the effective "filter cake" or remixed layer formed during the recovery phase lacked the long-term durability of the bentonite mixtures and was gradually degraded by the continuous cyclic loading. This late-stage degradation suggests the sealing layer appears stable and functional for a short period but is actually fragile and prone to failure over time under continuous stress, possibly due to lower erosion resistance. It is hypothesized that if a subsequent quiescent resting period were introduced, the suspended clay particles might re-deposit and fuse into the interface, potentially allowing the resistance to rebound and a new effective layer to establish. However, under continuous dynamic action, the S1 clay interface appears prone to progressive erosion and reduction in permeability.

It is interesting to point out that the sand-S1 clay mixture with high and low clay concentration tests reached a similar resistance time towards the end of the test, suggesting that an effective layer was formed with comparable characteristics in both cases after the damage of the original mixture layer. This is also observed in the sand-bentonite tests.

4.2.4 Sand – dredged mud test results (soft solution with 40 cm layer)

The experimental set-up for the sand-dredged mud mixtures utilized a 40 cm layer prepared at high and low mud concentrations, placed on top of the compacted sand base (Figure 4-21 and Figure 4-22). The dredged mud, characterized by its source of origin, contained sediment particles, organic matter, broken shells and root fragments, resulting in a dark, cohesive initial mixture structure. The high-concentration test was not successful and only lasted for about 6 hours. Small root fragments present in the mud obstructed the discharge outlet, causing a blockage. This led to an uncontrolled overspill event, rendering the measured data highly uncertain, as evidenced by the scattering and the abrupt vertical jump in accumulated water mass approximately 3.5 hours into the test. To mitigate this in the low-concentration test, a mesh filter was installed over the outlet valve. This modification successfully sequestered plant residues and prevented blockage, ensuring valid data collection over the entire test.

The final state of the low-concentration column reveals significant erosion of the upper bulk layer. Visual inspection revealed a stratified layer structure similar to the S1 clay cases: the column featured a turbid suspension of fine particles and organic residue in the upper section, following a transitional mixed zone where the sand fraction progressively increased. This structure ended with a consolidated effective layer at the interface with the base sand.



Figure 4-21. The initial setup of the test (based sand layer plus a sand-dredged mud mixture layer of 40 cm - high mud concentration) on the left and the intermediate state of the layers before the test failed on the right.



Figure 4-22. The initial setup of the test (based sand layer plus a sand-dredged mud mixture layer of 40 cm - low mud concentration) on the left and the final state of the layers after the test on the right.

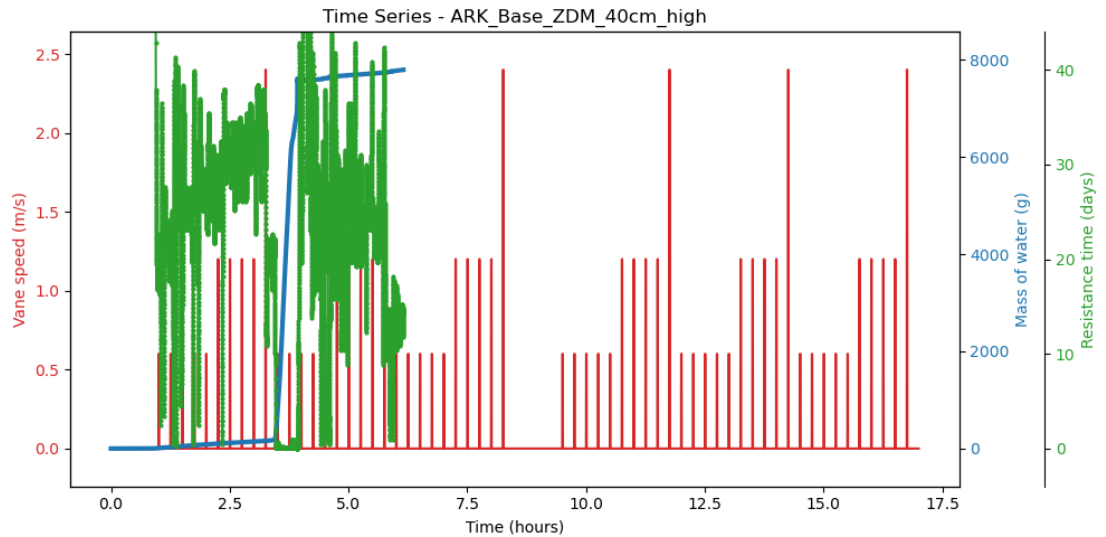


Figure 4-23. The measured mass of water during the test, the speed of vane rotation and the derived resistance time (base sand layer plus a sand-dredged mud layer of 40 cm with high mud concentration).

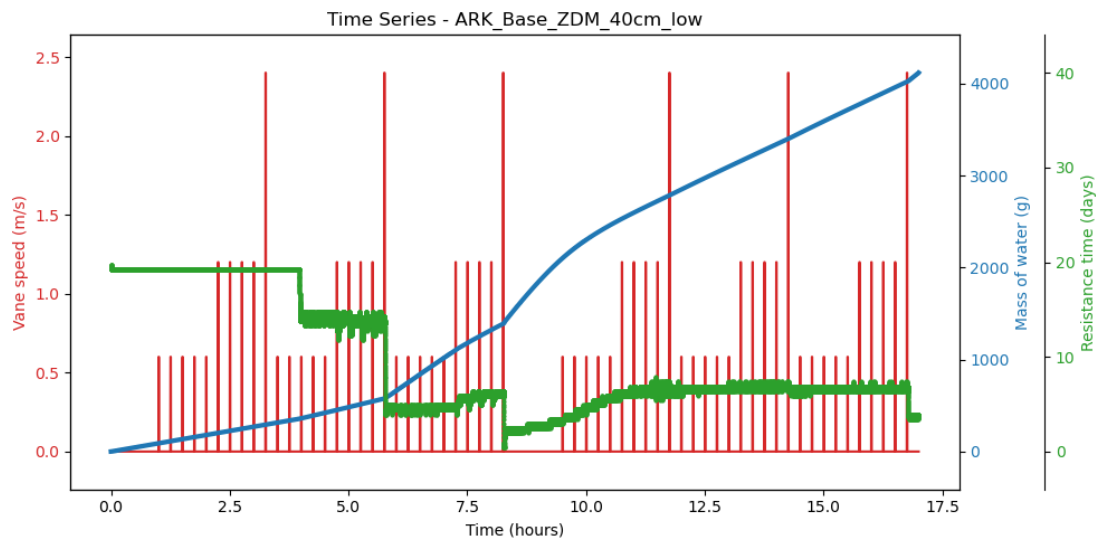


Figure 4-24. The measured mass of water during the test, the speed of vane rotation and the derived resistance time (base sand layer plus a sand-dredged mud layer of 40 cm with low mud concentration).

The time-series data for the low-concentration test (Figure 4-24) demonstrates that this mixture's sealing layer is dynamic rather than permanent. During the initial phase (0–4 hours), the layer exhibited high stability with a resistance time maintained at approximately 19 days, accompanied by a steady leakage rate. This suggests that the effective layer still had sufficient thickness sealing the bottom despite the onset of erosion at the upper section of the mixture layer. Between 4 and 8 hours, a stepwise reduction in performance was observed, with resistance time dropping to 13–14 days and later around 5 days, suggesting damages in the effective layer roughly after every 10th cycle of vane action. A critical failure event occurred after 8.5 hours when the vane speed peaked at 2.4 m/s, causing resistance to plummet to nearly zero and the water leakage rate to increase sharply, indicating significant erosion and failure of sealing under high shear. However, in the subsequent phase (8.5–17 hours), the material demonstrated a notable "self-repairing" capability; despite continued cycles of vane actions, the resistance time gradually recovered to approximately 7-8 days, indicating that the

effective layer was re-established and blocked the flow paths created during the high-stress event. However, this recovered state proved fragile. At the very end of the test (approx. hour 17), the re-introduction of the peak vane speed (2.4 m/s) caused the resistance time to decrease again. This confirms that the "healed" layer remains instable: while it can reorganize and seal during low-stress periods, it lacks the strength to withstand repeated high-intensity shear forces, leading to recurring degradation.

Note that after the second reduction phase at about 6 hours, there was a brief rebound of resistance time. It seems that there is an equilibrium resistance time (about 6-7 days) for this specific type of material under the specific dynamic loadings. Once the resistance time becomes lower than this value, the effective layer may rebuild itself before the peak vane speed (2.4 m/s). The resistance time cannot remain higher than the equilibrium value because the strength of the material cannot withstand the shear stress at the peak vane speed.

4.2.5 Sand – granulate test results (soft solution with 40 cm layer)

The performance of the sand-granulate material was evaluated using 40 cm mixture layers prepared at high and low concentrations (Figure 4-25 and Figure 4-26). Visual inspection of the final column states reveals that, similar to the other mixtures, the dynamic loading caused significant erosion of the upper layer. However, unlike the cohesive clay or mud, the granulate mixture, being a non-swelling, inactive material, appears to have undergone a segregation and sorting process. Fine particles were separated from the original mixture and suspended in the upper layer, followed by a transition layer where the sand fraction increased towards the bottom. However, at the interface, a layer of the sand-granulate mixture remained at the end of the test, functioning as the effective layer. This layer was notably thicker in the high-concentration test and thinner in the low-concentration test.



Figure 4-25. The initial setup of the test (based sand layer plus a sand-granulate mixture layer of 40 cm - high granulate concentration) on the left and the final state of the layers after the test on the right.

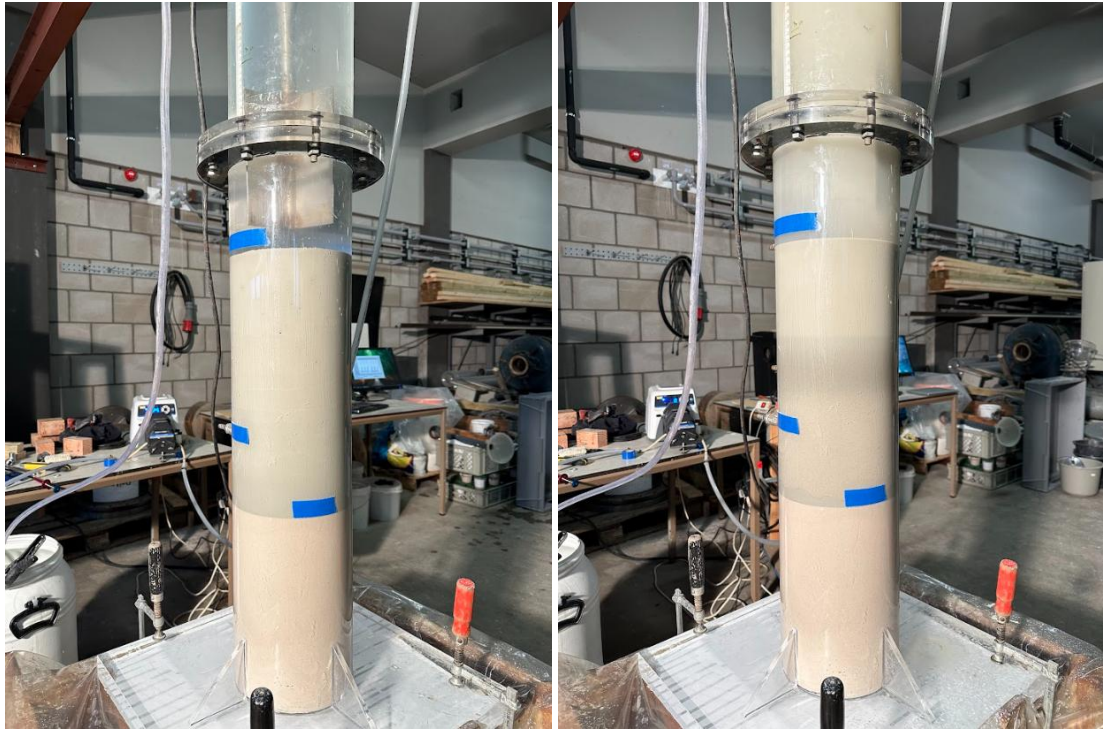


Figure 4-26. The initial setup of the test (based sand layer plus a sand-granulite mixture layer of 40 cm - low granulite concentration) on the left and the final state of the layers after the test on the right.

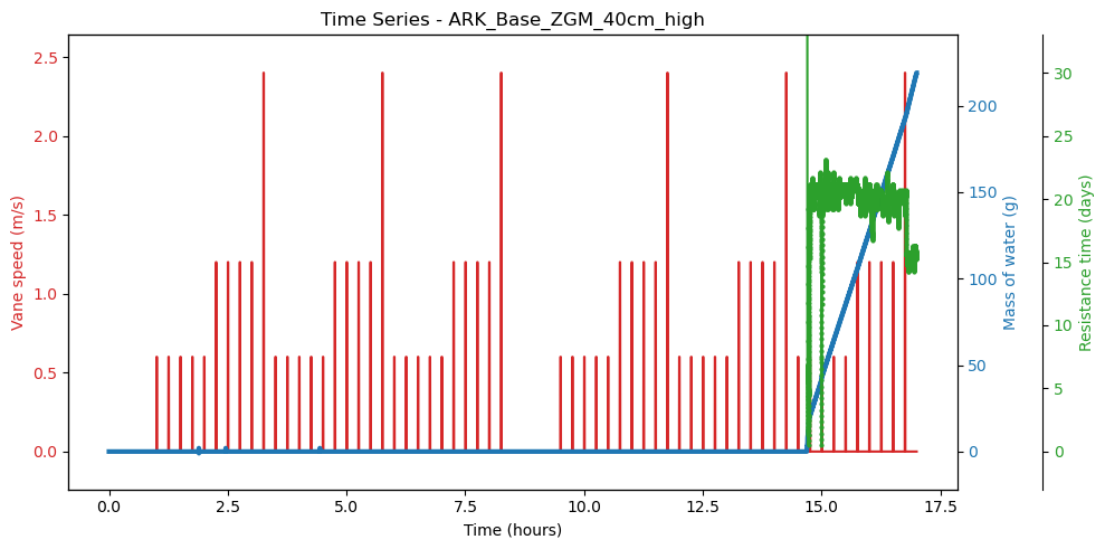


Figure 4-27. The measured mass of water during the test, the speed of vane rotation and the derived resistance time (base sand layer plus a sand-granulite layer of 40 cm with high granulite concentration).

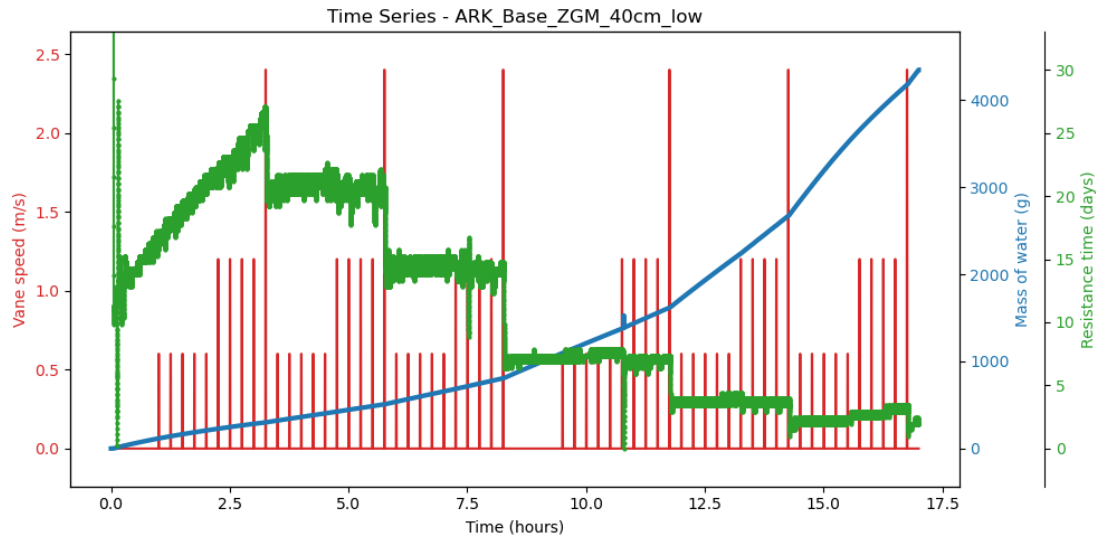


Figure 4-28. The measured mass of water during the test, the speed of vane rotation and the derived resistance time (base sand layer plus a sand-granulite layer of 40 cm with low granulite concentration).

The quantitative analysis of the high-concentration test presents a specific measurement artifact: the recorded water mass remains completely flat for the first 14.5 hours (Figure 4-27). This flat line segment is attributed to the electronic scale's drift compensation mechanism, which likely masked a slow, steady leakage rate that fell below the detection threshold. This issue was avoided in the low-concentration test, where the initial accumulation of filtrate (3–4 grams) successfully activated the weighing system, providing a reliable baseline for behavioural analysis (Figure 4-28). Assuming the hydraulic conditions are consistent, the high-concentration mixture likely followed the pattern of the low-concentration case but with enhanced resistance due to the ~44% higher granulite content increasing the mixture strength.

For the low concentration granulate test, initially (0–3 hours), under low to medium vane speeds (0.6–1.2 m/s), the resistance time increased steadily, peaking at over 25 days. This indicates a 'self-weight consolidation' phase where the particles in the effective layer packed tighter under hydraulic pressure, while the upper part of the mixture likely acted as a temporary protection layer against erosion. As vane actions continued, a distinct multi-step reduction in resistance was observed. Similar to the stepwise permeability change seen in the clay and dredged mud tests, the granulite resistance dropped sharply with each occurrence of the peak vane speed (2.4 m/s), suggesting the destruction of structural layers. The most significant finding occurred after the peak velocity event at 8.5 hours, where resistance collapsed to 7.5 days and, crucially, did not recover during the subsequent resting phase. Unlike the other materials which exhibited 'self-repairing' capabilities, the granulite resistance remained low. This confirms that without cohesion or swelling capacity, damage to the granulite seal is permanent; once the particle matrix is physically disrupted, it cannot easily reorganize to seal the flow paths. At the end of the low concentration granulate test, the resistance time is only 3–4 days and still decreasing after each 2.4 m/s vane action. For the high concentration granulate test, the end resistance time is 15 days, but also still decreasing after a 2.4 m/s vane action.

The recovery behaviour observed in these column tests might be influenced by the mixing of granulite with sand. Pure granulite would probably exhibit different behaviour under hydraulic loads, but as explained in Section 2.1, pure granulite is not included in the 2025 test series because in the 2019 tests (Deltares 2019a) water was leaking at the interface granulite-plexiglass of the column tests, which influenced the results significantly.

4.2.6 Materials with a protection sand layer on top

This section provides the results for three tests with a protection sand layer on top of the sealing layer as a stratified “sandwich” configuration. In this arrangement, the active sealing layer was placed in between a 30 cm compacted base sand layer and a 30 cm top sand layer. The primary function of the top sand layer was to act as a protective buffer, shielding the cohesive material from the direct hydrodynamic shear and erosion caused by the rotating vane.

Three specific materials were tested within this category:

- Premixed ZBM (8 cm thick).
- S1-clay (10 cm thick, mixture density of 0.5804 g/cm³).
- Dredged mud (10 cm thick, mixture density of 0.7061 g/cm³).

Visual inspection of the final states (Figure 4-29 to Figure 4-31) indicates that the interface between the sealing layer and the base sand layer stayed sharp and intact, also at the end of the test after many vane events. Only the bottom 1-2 cm of the original 8-10 cm sealing layer remained in position. The majority of the sealing layer eroded during the test and the fine particles of the sealing layer (bentonite, clay or mud) escaped from their original layer during the multi-stage erosion events and went in suspension due to their lower settling velocities. Directly above the remaining 1-2 cm of the original sealing layer a sand-dominant layer is found, followed by a thin mixed layer of sand and bentonite, clay or mud. The layer structure was similar to what we observed in the previous tests, but the sealing layer was preserved in a better state, suggesting the top sand could dampen the forces by the vane actions and better protect the effective layer beneath it.



Figure 4-29. The initial setup of the test (an 8 cm premixed ZBM layer in between a 30 cm base sand layer and a 30 cm top sand layer) on the left and the final state of the layers after the test on the right.



Figure 4-30. The initial setup of the test (a 10 cm S1 clay layer in between a 30 cm base sand layer and a 30 cm top sand layer) on the left and the final state of the layers after the test on the right.



Figure 4-31. The initial setup of the test (a 10 cm dredged mud layer in between a 30 cm base sand layer and a 30 cm top sand layer) on the left and the final state of the layers after the test on the right.

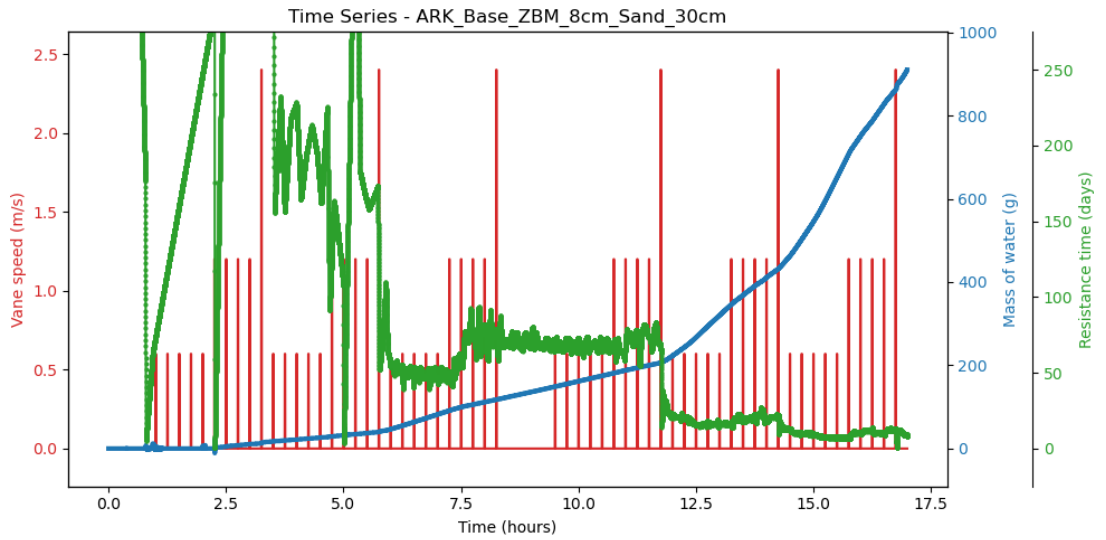


Figure 4-32. The measured mass of water during the test, the speed of vane rotation and the derived resistance time (an 8 cm premixed ZBM layer in between a 30 cm base sand layer and a 30 cm top sand layer).

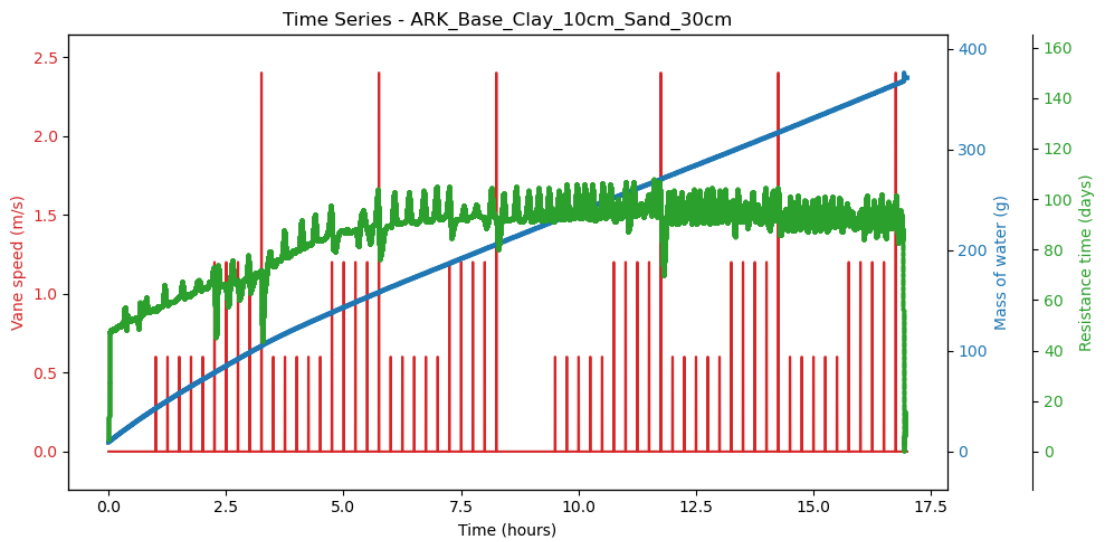


Figure 4-33. The measured mass of water during the test, the speed of vane rotation and the derived resistance time (a 10 cm S1 clay layer in between a 30 cm base sand layer and a 30 cm top sand layer).

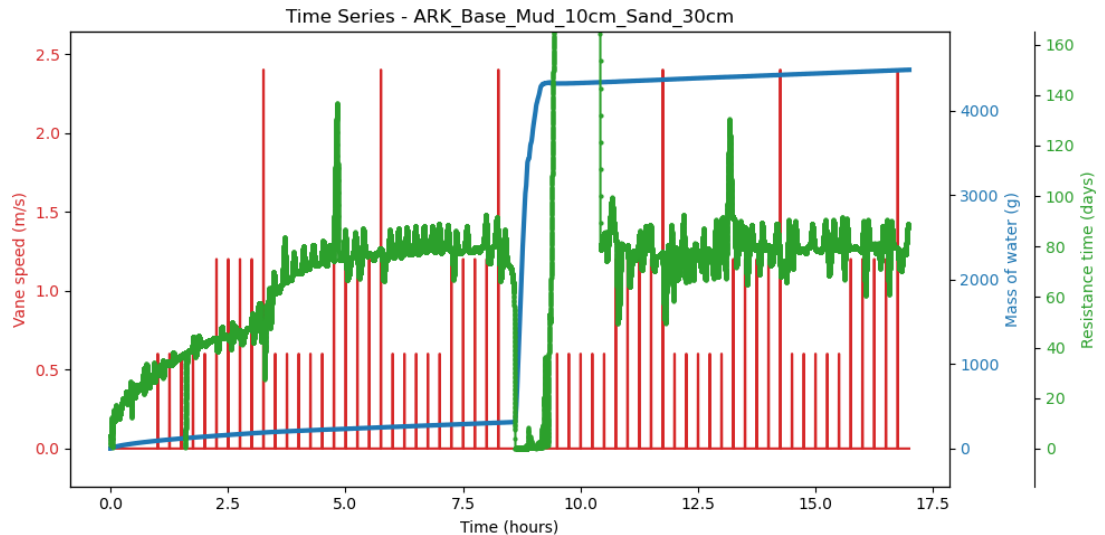


Figure 4-34. The measured mass of water during the test, the speed of vane rotation and the derived resistance time (a 10 cm dredged mud layer in between a 30 cm base sand layer and a 30 cm top sand layer).

The time-series data from the "sandwich" configuration tests reveals a distinct divergence in the performance between the ZBM material and the pure cohesive sediments such as S1-clay and dredged mud (Figure 4-32 to Figure 4-34). The ZBM test demonstrated a behaviour consistent with the previous mixture experiments, with a lower resistance the more high vane speed actions have been completed, resulting in a moderate resistance time of approximately 10 days at the end of the test. This consistency suggests that the sand-bentonite matrix does not undergo dramatic structural evolution or significant secondary consolidation under these loading conditions, it establishes a functional but permeable steady state similar at the end of all the ZBM tests.

In contrast, the pure S1 clay and pure dredged mud tests achieved significantly higher sealing capacities, with resistance times peaking in the range of 80–90 days. It is noted that the dredged mud dataset includes an operational artifact around the 9-hour mark, where outlet clogging caused a temporary overspill, yet the overall trend remained valid. During the tests, both materials showed a consolidation-stabilization pattern, with no obvious degradation in the performance. The ability of these materials to generate such high resistance despite having only a 1–2 cm effective layer remaining indicates a fundamental change in their physical state. Unlike the ZBM, the pure cohesive fines likely underwent rapid consolidation, transforming into a high-density "filter cake" characterized by high yield strength and extremely low permeability. This likely happened in the last 1-2 cm above the base sand layer in the first 5-8 hours.

The final layer structure in these "sandwich" tests closely resembles that of the previous 'mixed sand-material' tests. This suggests that the vane actions created an affected zone where erosion, sediment sorting, and remixing drive the system toward a common equilibrium structure, which was less influenced by their initial configurations (sand and fine particles was mixed or separated). Once the vane mobilized the sediment (typically within a 30-second window during high-velocity cycles), sediments were eroded, fine particles and coarser sand were separated based on settling velocity. Coarser sand particles settled rapidly to form the lower skeleton, while fine cohesive particles remained in suspension longer, creating the observed stratification. The main difference may lie in the characteristics of the remaining effective layer below the "effected zone", at the interface with the base sand layer. In the "sandwich" tests, the remaining material was largely in its pure state (although consolidation may have enhanced its initial strength and effectively reduced permeability), whereas in the

“mixed sand–material” tests, the remaining layer was still a sand–material mixture and may have consolidated less due to the presence of a load-bearing sand skeleton.

The “sandwich” and the “mixed sand-material” configurations both showed that the top sand layer functioned as a buffer, damping the hydrodynamic forces generated by the vane actions (no matter it was placed intentionally from the beginning or emerged due to erosion-segregation-sorting). Erosion ceased at the depth where the hydrodynamic shear stress was damped sufficiently to be balanced by the material's strength. Below this critical depth, the effective layer remained stable. Under the influence of hydraulic pressure, a “filter cake” was formed at the interface with the base sand. This confirms that the long-term sealing capacity is not provided by the bulk thickness of the installed material, but by this thin, consolidated layer usually just within a 1-2 cm.

4.2.7 ZBM with a protection gravel layer on top

The final experimental configuration evaluated the efficacy of an armour layer made of gravels in mitigating erosion. In this setup, an 8 cm premixed ZBM layer was installed over the standard 30 cm sand base, followed by the application of a protective gravel layer (approximately 10 cm thick, with an average diameter of 5 cm) dropped from a height of 50 cm above the surface of the ZBM layer. Gravel with a diameter of 5 cm is considered stable for a ship return flow of 1.2 m/s, following from the Rock Manual (CIRIA 2007) formula. Most of the gravel sank into the ZBM layer immediately, displacing the ZBM material upwards within the column. The remaining gravel stacked on top, forming a visible 3 cm thick layer (Figure 4-35). It may indicate that some of the gravel did not sink deep enough to reach the base sand layer. This can be attributed to the ZBM's behaviour as a viscous paste with internal strength, which hindered the gravel's penetration. Additionally, the friction at the column wall may have contributed to this resistance.

Unfortunately, the experiment was prematurely terminated at the 14-hour mark due to a catastrophic mechanical failure (Figure 4-35). As the underlying ZBM layer experienced gradual erosion under the dynamic loading, the stability of the stacked gravel was compromised. During a peak velocity cycle, the high shear forces remobilized certain gravel stones, resulting in a high-energy impact between a rapidly rotating vane blade and a gravel stone. This collision shattered the acrylic column wall, causing an immediate flushing of water, sediment and gravels. Despite this violent end, visual inspection of the column showed that a distinct ZBM layer remained intact on top of the base sand. This suggests that, prior to the mechanical failure, the gravel armour successfully dampened the shear stress and protected the effective sealing layer from the washout observed in the unprotected tests.



Figure 4-35. The initial setup of the test (an 8 cm premixed ZBM layer in between a 30 cm base sand layer and a 10 cm gravel on top) on the left and the final state of the layers after the test on the right.

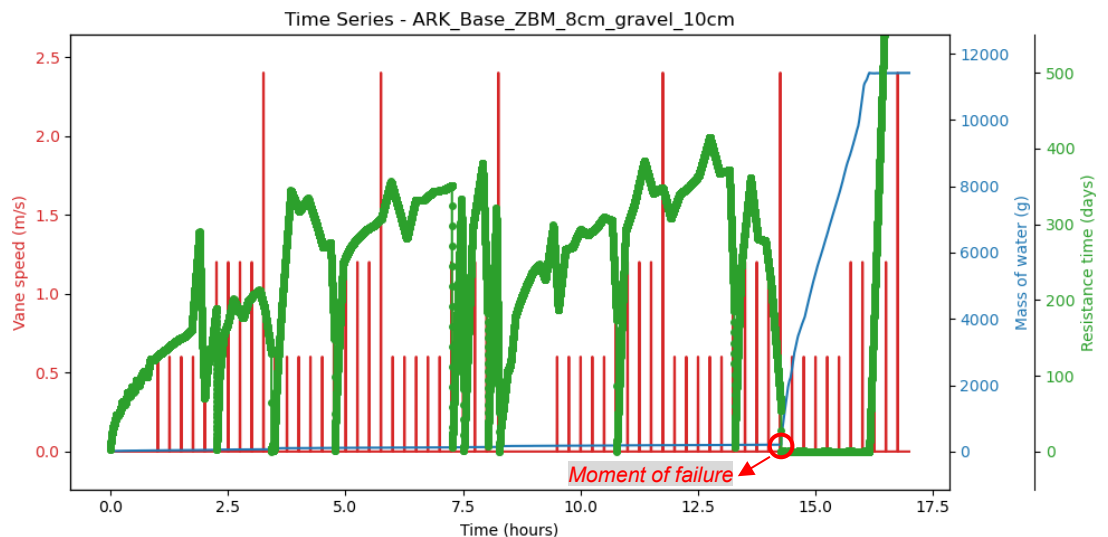


Figure 4-36. The measured mass of water during the test, the speed of vane rotation and the derived resistance time (an 8 cm premixed ZBM layer in between a 30 cm base sand layer and a 10 cm gravel on top).

The quantitative results for the gravel-protected ZBM configuration reveal an overall performance characterized by superior sealing capacity but with large variations as well (Figure 4-36). Prior to the failure of the test at the 14-hour mark, this configuration demonstrated the highest resistance time observed across the entire experimental program, with resistance values frequently peaking between 250 and 300 days. This represents an order-of-magnitude improvement over the unprotected or sand-covered ZBM tests in this program (typically ~10 days). However, the time-series data also highlights substantial variation; the resistance values exhibit large oscillations, particularly during and immediately following high-velocity vane

events. This variance is attributed to the complex hydro-mechanical interaction at the interface: localized erosion of the ZBM occurred within the spaces between the gravels, while the stones themselves underwent rearrangement and mobilization under high flow velocities, which also affected the integrity of the ZBM layer in the vicinity. Consequently, while the gravels significantly enhances the shear stress resistance by shielding the effective layer, the system remains sensitive to the stochastic configuration of the gravel armour and the intensity of the shear forces.

5 Discussions and conclusions

The primary objective of this study is to test a range of soft solutions to make a canal bed, for example on the ARK canal bottom, less permeable. Static soil CST permeability tests have been performed as well as 14 column tests with periodic hydraulic loading with a vane. Despite challenges during execution, the test campaign yields valuable insights into the behaviour of the different materials. In the following sections, first the main conclusions from the CST tests are provided (5.1 and 5.2), followed by the behaviour of the different solutions under dynamic loading in the column tests (5.3). Reflections on the test setup are provided (5.4), and this section ends with practical conclusions for application on ARK (5.5). In the next chapter recommendations for follow up research are made.

5.1 Mechanisms of sealing and performance grading from the CST tests

The performance regarding the hydraulic resistance time of the tested mixtures exhibits a vast divergence in efficiency, a phenomenon best explained by the fundamental physical and chemical mechanisms governing flow restriction in each material type. Based on the Capillary Suction Time (CST) results under static condition, the performance grading, bentonite > clay > mud > granulite, is driven by the transition from active chemical swelling and cohesion to passive physical pore-filling.

- Sodium activated bentonite as present in ZBM and OCMA bentonite (active swelling): This material contains montmorillonite clay minerals that chemically interact with water, absorbing it into their platelet structure. This hydration causes significant expansion, creating a tight, cohesive gel that actively blocks pore spaces. Because the material expands to many times its dry volume, a relatively small solid mass is sufficient to effectively seal the voids between sand grains.
- Clay (cohesion): Clay functions through plasticity and physical cohesion (flocculation). Unlike bentonite, it does not significantly expand to fill voids; rather, clay particles bond and physically occupy the interstitial spaces. Consequently, creating an effective seal requires a higher solid mass to physically plug the majority of the pore volume compared to Bentonite.
- Dredged mud (heterogeneous filling): In dredged mud, the cohesive sediment functions in a similar way as clay, which means it may flocculate and form matrix that enhances its internal structure. But the presence of non-sealing impurities (organic matter, roots, shells, sand, non-flocculating mud) dilutes the effective cohesive content. These impurities contribute less or not to sealing and may create preferential flow paths or micro-channels. Therefore, a larger total volume is required to ensure sufficient fine particle availability for a continuous barrier.
- Granulite (inactive packing): Granulite acts as a fine silt or inert filler with negligible chemical interaction with water (no swelling). Its sealing mechanism is purely physical packing—relying on the jamming of fine particles into the sand's voids. Lacking the "tightening" effect of gel formation, this material requires higher concentrations to reduce permeability compared to the other three substances. The observed lack of cohesive behaviour might be influenced by the mixing of granulite with sand. Pure granulite would probably exhibit different behaviour, but pure granulite is not included in the 2025 test series because in the 2019 tests (Deltares 2019a) water was leaking at the interface granulite-plexiglass of the column tests, which influenced the results significantly.

5.2 Overview of the column test results

The calculated filtration velocity and the resistance time based on the data in the last hour of each test are summarized and shown in Tabel 5-1. These results are supposed to be approximations to the performance of each soft solution after stabilizing under the dynamic vane actions. The highest vane speed of 2.4 m/s in the column tests is 1.7x higher than the highest measured ship-induced flow velocity, but the corresponding bed shear stress from the vane corresponds to the highest measured shear stress in the 9-day field campaign in ARK (Deltares 2025a). Given the limited measurement period of 9 days in the field campaign it is possible that incidentally higher ship-induced flow speeds occur in the ARK. The occurrence of the high shear stresses in the vane protocol is more frequent than in the field measurements. Hence, the applied vane protocol is considered to be representative, but on the conservative side for ARK conditions.

Note that for incomplete or failed tests (i.e., Test #7 and Test #14), where the layer did not endure the full test duration, the data represent performance at an earlier stage rather than a stabilized state.

Overall, the findings are as follows.

- The most notable finding is the significant performance disparity between the 'homogeneous mixture' and 'sandwich' configurations for S1 clay and dredged mud (tests 12, 13 vs tests 5-8). This difference is likely driven by the composition of the effective layer formed 1–2 cm above the base sand. In the 'sandwich' configurations, where this effective layer consists of pure clay or mud, the consolidation process appears capable of significantly enhancing the sealing properties. In contrast, this enhancement was not observed when the effective layer consisted of sand-clay or sand-mud mixtures.
- In contrast, the sand-bentonite mixtures (including premixed ZBM and sand-OCMA bentonite) demonstrated remarkably consistent results across nearly all configurations (tests 1-4 and 11), with the notable exception of the gravel protection layer case (test 14). This suggests that under dynamic vane loading, the sand-bentonite layer erodes and mixes with the surrounding sand, eventually evolving into the same equilibrium structure independent from the initial bentonite layer configuration. This implies that the sealing mechanism of bentonite may differ from that of clay and mud. We hypothesize that bentonite acts as a sealant by infiltrating the pore structure at the base sand interface, whereas the performance of clay and mud depends largely on the integrity and state of the bulk material itself. Consequently, for clay and mud, the consolidation and composition of the effective layer play the major role in sealing capability. The presence of the gravel protection layer seems drastically altering the hydrodynamic conditions around the ZBM material and preventing the failure modes in the effective layer seen in other setups.
- Tests with sand-granulite mixtures appears to be highly sensitive to the granulite concentration. The "high concentration" mixture (test 9) performed decently (resistance time of 20.1 days), but the "low concentration" (test 10) dropped significantly to 3.1 days (the lowest in the entire test series). This may indicate a sharp threshold for effectiveness with this material, or the "high concentration" mixture may take a longer period to degrade (longer than the testing time). Perhaps a thin layer of pure granulite would also function well, but in present setup that could not be tested.

Table 5-1. Overview of the column test results. The filtration velocity and the corresponding resistance time is computed based on the measured data during the last hour of the tests. Percentages represent the relative solid volume fractions of each soil type in a mixture (both soil types adding up to 100%) .

#	Description	Filtration velocity ($\times 10^{-8}$ m/s)	Resistance time (day)
1	Top ZBM double layer 8 cm	166	11
2	Top ZBM thin layer 4 cm	193	9
3	Soil improvement with homogeneous sand-bentonite mixture with ~2.5% OCMA bentonite and ~97.5% sand (but lower concentration than a pure ZBM layer)	164	11
4	Soil improvement with homogeneous sand-bentonite mixture with ~1.5% OCMA bentonite and ~98.5% sand	186	9
5	Soil improvement with homogeneous sand-clay mixture with ~18% S1 clay and ~82% sand	490	4
6	Soil improvement with homogeneous sand-clay mixture with ~14% S1 clay and ~86% sand	400	4
7	Soil improvement with homogeneous sand-dredged material mixture with ~38% dredged material and ~62% sand ⁴	99	18
8	Soil improvement with homogeneous sand-dredged material mixture with ~26% dredged material and ~74% sand	259	7
9	Soil improvement with homogeneous sand-granulite mixture with ~70% granulite and ~30% sand	86.2	20
10	Soil improvement with homogeneous sand-granulite mixture with ~49% granulite and ~51% sand	569	3
11	8 cm ZBM with 30 cm sand on top	179	10
12	10 cm clay with 30 cm sand on top	19.6	89
13	10 cm dredged material with 30 cm sand on top	21.6	81
14	8 cm ZBM with gravel layer on top as extra protection against ship loading ⁵	7.84	221

⁴ The test was not complete due to the blockage of the outlet of water. The result was calculated based on the data in the last hour before the terminal of the test, which excluded the data artifacts caused by the water overspill.

⁵ The test failed due to the breakage of the column. The result was calculated based on the data in the last hour before the moment of failure.

5.3 General behaviour of soft solutions under dynamic loading in the column tests

Despite the differences in material composition, a common behavioural pattern was observed across the tested materials (bentonite, clay, dredged mud and granulite). The time-series data reveals a distinct three-phase response to dynamic loading:

- Initial consolidation: In the first 2–3 hours, the mixture undergoes a consolidation phase where resistance increases, often aided by the protective function of the upper sediment layer.
- Stepwise erosion: Under repeated dynamic loading, a "step-down" in resistance time is observed. This degradation is strongly correlated with the peak flow velocities (2.4 m/s) in the test, suggesting that extreme shear events drive the destruction of the sealing layer. Erosion-segregation-sorting process produced a consistent layered structure in the majority of the tests, resulting in a transition from dilute suspension of fine particles, to mixed sand-fines layer with sand fraction increases downwards, to a remaining effective layer at the interface with the base sand. The thickness of the mixed sand-fines layer may change with different flow velocity because a specific flow speed may mobilize and remix a certain thickness.
- Self-repair and stabilization: A crucial recovery phase occurs during resting periods. Provided there is an abundance of suspended fines acting as a material reservoir, these particles re-sediment and fuse into the interface, stabilizing the effective layer for the remainder of the test.

It is worth noting that, for the ZBM and sand–OCMA bentonite mixtures, no significant degradation of resistance time was observed toward the end of the tests. This indicates that the effective layer remained stable after 17 hours. In contrast, for the other sand-material mixtures, degradation near the end of the tests was frequently observed, suggesting that erosion and self-repair phases may recur under sustained dynamic loading. Although such systems may still converge to an equilibrium resistance time provided sufficient sealing material is available, a periodic degradation–recovery pattern may persist.

The investigation into structural configuration demonstrated that a protective top layer could significantly enhance the performance by dampening hydrodynamic shear forces. Tests utilizing a "sandwich" configuration (top sand layer) revealed a phenomenon of hydrodynamic convergence, where the protective sand mobilized and mixed in-situ with the underlying material; however, by dissipating vane energy, it preserved a robust interface that allowed pure cohesive materials (clay and mud) to consolidate into high-density "filter cakes" with superior resistance (80–90 days) compared to pre-mixed equivalents. Furthermore, the application of larger gravel armour yielded the highest peak resistance of the study (250–300 days) by effectively shielding the cohesive seal, yet this setup proved operationally volatile, as the remobilization of stones (destabilization possibly due to the erosion of surrounding ZBM under high velocity) may lead to large variations in the resistance time and possibly a less predictable performance in certain local areas.

A critical synthesis of the experimental results also reveals that a protective upper layer consisting of coarser sediment is a universal feature of stable sealing systems, originating either from initial engineering or hydrodynamic evolution. In the "sandwich" configuration, this protection was explicitly designed, with the top sand or stone layers serving as an immediate physical buffer to dampen vane energy. However, a functionally identical mechanism emerged spontaneously in the pre-mixed tests (ZBM, granulite, and mixtures) through segregation and sorting. As the initial bulk mixture eroded, hydrodynamic forces washed out the fines while the coarser sand fraction rapidly settled, forming a graded, sand-dominant transition zone. Whether artificially placed or naturally evolved, this coarse sediment buffer performs the same critical function: it dissipates the shear stress of the overlying water column while still can

remain in the system over a long-term, shielding the delicate thin "effective layer" at the base interface and allowing it to consolidate into a functional filter cake under hydraulic pressure.

5.4 Reflections on test setup

In the column test a pump ensures a constant water level above the soil by pumping in water from a bucket and an overflow from the column which spills the excess water back into the bucket. The pump capacity is such that it can recirculate the complete water volume in the column in 90 minutes. Depending on the fine sediment concentration in the water at the top of the column flowing out via the overflow this means that slowly the amount of fine sediment reduces during a test as it is pumped into the bucket where it deposits. Without measurements of the time development of fine sediment concentration in the overflow water during and after each vane action it is difficult to assess how much fine sediment this concerns. However, it is expected that the amount of fine sediment flowing out via the overflow is limited because each vane action only lasts 30 seconds after which there is a pause of 14.5 minutes in which the water is not stirred and sediment can slowly settle. This leads to a surface layer with low concentration and the overflowing water is taken from the top millimetres of the water layer in the column. Additionally, in the real situation of the ARK a slow reduction in amount of fine sediment being present in the shipping lanes, where sealing is needed the most, is also expected to occur because of lateral redistribution of fine sediment by the passing ships. Hence the recirculation of water in the column tests is not expected to significantly influence the usability of the outcomes for the ARK significantly. As the long-term loss of fines in critical locations by the lateral redistribution of fines in ARK probably is more than the water recirculation in the column tests the influence of the lateral redistribution of fines on the functioning of a soft solution in a canal like ARK requires further investigations, see the recommendations.

The vane action is designed such that the tip speed and shear stress values are representative for the ship return flow at ARK. Also, the duration and frequency of the vane actions is designed in line with measured ship parameters in ARK. However, the aspects of lateral distribution of fines, discussed above, and spatial heterogeneity and turbulence of the flow field from a vane are different from ship loads. In the column experiments it was observed that higher bed shear stress near the walls led to a thinner effective layer in the outer regions compared to the inner region of the column. While loss of material was inevitable during the early stages of erosion, the thickness of this outer region often stabilized upon reaching equilibrium. This suggests a two-stage process: first, the effective layer is eroded to a specific depth; second, the resulting change in bed geometry reduces the localized shear stress, allowing the system to stabilize. During this later phase, the layer can 'self-heal' with very small amounts of fine material, preventing further degradation. As the permeability is dominated by the zones with highest permeability and the zones near the wall comprise the highest area in the column, the test results are expected to be dominated by the thinner effective layers near the walls, making the presented vane tip velocity and shear stresses the governing parameters. In the recommendations flume tests and a pilot test are recommended to have a more representative hydrodynamic loading from actual ships instead of a vane mimicking ship influence.

Comparing 2019 and 2025 test setup:

- In comparison with the 2019 column tests (Deltares 2019a), the 2025 bentonite column tests result in lower resistance values of about 8-10 days at the end of each test than according to the 2019 column tests in which 5-10 cm ZBM achieved resistance values of ~40-80 days.
- Periodic vane action is used in the column tests to mimic the influence of passing ships. The applied vane protocol is conservative regarding the frequency and intensity of the loads. Especially the six peak vane actions of 2.4 m/s in the test, which are 1.7x the flow speed measured for passing ships in ARK (Deltares 2025a), turn out to reduce the

sealing properties of the tested soft solutions considerably. On the other hand, in the 2019 column tests ZBM could withstand vane actions up to 3.6 m/s without strong reduction in hydraulic resistance.

- An important difference between the 2025 and the 2019 tests is the resting period without vane action. In 2019 the ZBM layer was given 19 hours resting time before the vane started and in the 2025 tests there is only 1 hour resting time without vane action. Sufficient resting time without vane action (passing ships) turns out to be crucial for the functioning of a soft solution.

Hence this comparison between the 2019 and 2025 test setup highlights that for the proper functioning of soft solutions it is not only the intensity of the hydraulic load that matters, but also how often loads occur and the duration of the in-between resting periods. In follow up tests it is advised to investigate the influence of different vane action protocols in combination with a longer resting time. This can provide valuable input in assessing the necessity of a temporary pause in shipping during placement of ZBM or other soft solution in the ARK and into the robustness of soft solutions to variation in shipping loads.

5.5 Practical conclusions for ARK

Some, but not all, tests with different soft solutions reach the target resistance of ~45-90 days during the initial phase of the test where vane action is not so strong, but almost none reach the target resistance of ~45-90 days at the end of the test. Please note that the applied vane protocol is conservative regarding the frequency and intensity of the loads. Especially a repetition of several 2.4 m/s vane actions proves to reduce the resistance significantly (9-11 days). Hence, for a functioning soft solution in the ARK it must be given sufficient resting time after placement, more than in these tests, before significant hydrodynamic loads from ships start. The comparison of the 2019 and 2025 column tests hint at a required resting time of approximately a day for ZBM, but more research is needed on this aspect.

The only three tested solutions that reach the target resistance of ~44-88 days at the end of the test are the 10 cm clay and 10 cm dredged mud layer topped by a 30 cm sand protection layer and ZBM covered with gravel. Hence, placing a covering layer on top of a soft solution to protect it against erosion is beneficial for its functioning after periodic hydraulic loading. For the application of gravel as protection layer more research is required about the functioning of the underlying soft solution after movement of individual rocks during a ship passage.

Of all the tested soft solutions bentonite shows the highest potential as this has the benefit of active swelling providing a certain reduction in permeability with the lowest amount of solids from all tested solutions. The active swelling behaviour of bentonite also gives it an advantage in recovery potential as only a little amount of bentonite flowing into a damaged zone with high permeability can fix its functioning. In combination with a 30 cm top layer of sand, clay and dredged mud resulted in a higher hydraulic resistance than ZBM because clay and mud build up a stronger, more erosion resistant layer. That is a benefit of regular clay and mud over bentonite.

All tested soft solutions have the potential of erosion for the hydrodynamic loads from passing ships. Safest design is a soft solution that is stable for all (ship) loads that can occur. For the tested soft solutions, only the combination of a soft solution with sufficient covering layer of sand and/or gravel can achieve this, or (not tested) perhaps without covering layer, but with a longer initial resting time. In case a stable soft solution is not achievable, another way to get an effective solution is a design that allows for temporal erosion and has sufficient recovery capacity after each erosion event. Hence, there are three important criteria for a well-functioning soft solution: 1) reduction of permeability; 2) stability; 3) recovery potential. Bentonite performs best for aspect 1) and 3), because of its active swelling behaviour. Clay

and mud covered with sand build up a stronger layer and therefore perform better in the column test for aspect 2) than bentonite. It is the combination of the three aspects that in practice will provide the best functioning solution. Follow-up tests are recommended in the next section to investigate the three aspects in more detail and with this information identify the best functioning solution for ARK.

6 Recommendations

Present tests with dynamic loading involve many physical processes, such as consolidation, erosion and sediment-sorting, filtration under hydraulic pressure and rheology. For future work, it is recommended to focus on a smaller number of the most promising solutions and to complement these tests with more detailed measurements and sampling aimed at improving the understanding of the physical mechanisms.

The applied vane protocol in the 2025 tests is conservative regarding the frequency and intensity of the loads. In follow up tests it is advised to vary the hydraulic loading intervals and intensity from present test to find out how this influences the hydraulic resistance of soft solutions. It is also recommended to vary the resting time and assess its influence on the functioning of the soft solutions. In the ARK there is always a background current of nearly 5 cm/s. Hence, it is recommended to do a test in which ZBM is placed with a background current of 5 cm/s to investigate how this influences the resting that ZBM needs. It is also recommended to investigate the influence of different thickness of a sand cover layer on top a soft solution to identify the required layer thickness to keep the full original soft layer intact for different hydrodynamic conditions. In case a gravel cover layer is considered to be a viable option, then follow up research on the functioning of the ZBM after movement of the individual gravel pieces under hydrodynamic loads is recommended.

Present tests focussed on the overall behaviour of the different soft solutions. In follow up tests it is recommended to include more detailed physical measurement like the settling velocity of the mixtures; strength measurements of the different solution mixtures; measurements of the sediment sorting and resulting stratification profile under dynamic flow conditions; detailed measurements of the solid concentration and porosity and stresses in the thin layer that actually provides the sealing.

Present tests did not focus on the placement operations of the soft solutions. Different placement procedures, for example with lower costs or less hindrance for shipping or jetting into soil, can be tested in a flume test. Spatial redistribution of soft material by passing ships or background current is an important aspect for its functioning in practice in a canal like ARK, but is not included in present test setup. A column test is not suited to test these aspects, but flume tests are more suitable for this aim. Those flume tests can be performed in a smaller flume of 0.7 m high, or on a nearly one on one scale in the big water-soil flume of 2.5 m deep.

There are plans for a field pilot with ZBM in ARK. That is very positive, as in such field pilot the functioning and processes can be monitored for the 'real' conditions. It is recommended to not only measure the resulting resistance of the ZBM layer in the ARK under influence of passing ships, but also measure the erosion and deposition and spatial redistribution processes during and after passing ships in sufficient detail. It is possible that over the limited duration of such pilot the measured resistance of the ZBM layer does not change over time, but that in the longer term a slow deterioration of its functioning is occurring. Only when the processes responsible for a potential slow deterioration are measured during the pilot, insight is obtained in its long term functioning as well as the need for periodic reapplication of ZBM.

7 References

- Chassagne, C., van Kan, P.J.M. (2023). CEGM2000 Sediments, sludges and soils - Settling and dewatering. Lecture notes. Delft University of Technology. Delft, The Netherlands.
- Deltares (2019a), Arno Talmon, Afpleistering kanaalbodem - experimenteel onderzoek, Deltares, 11203424-002-ZKS-0002, maart 2019.
- Deltares (2019b), Arno Talmon, Beslibbingproef kanaalpand WGG t.b.v. project - Opwaardering Twentekanalen, Deltares, 11204174-000-ZKS-0002, december 2019.
- Deltares (2020), Arno Talmon, Geotechnische en geochemische proeven t.b.v. Twentekanalen, Deltares, 11205061-000-ZKS-0002, 6 april 2020.
- Deltares (2022), Lynyrd de Wit en Luka Jaksic, Gel barriers in the Port of Rotterdam, Analysis of the hydrodynamics, sediment transport and stability, Deltares, 11207279-000-ZKS-0001, 15 November 2022
- Deltares (2024), Arno Talmon, Verslag deelproject 1.2 - ARK kanaalbodem erosie en doorlatendheid, Deltares, 11210303-019-GEO-0001, 24 december 2024.
- Deltares (2025a), Analyse metingen scheepvaart Amsterdam-Rijnkanaal Maatregelen ter reductie wateroverlast langs kanalen - SITO Programmasubsidie IenW 2025, 11211511-026-GEO-0001 (concept november 2025).
- Deltares (2025b) INF14 Maatregelen ter reductie wateroverlast langs kanalen - Korrelverdelingen top 1e watervoerende pakket langs ARK, 11211511-022-GEO-0002 (nov 2025).
- Geolab Wiertsema (2025). Geotechnisch laboratorium onderzoek - Zandmonster ARK, VN-88428-1, 10 april 2025, Geotechnisch laboratoriumonderzoek Zandmonster ARK VN-88428-2 | 24 juni 2025.
- Gray, N. F. (2015). Capillary suction time (CST). In *Progress in filtration and separation* (pp. 659-670). Academic Press.

Huisman, M., van Kesteren, W. G. M. (1998). Consolidation theory applied to the capillary suction time (CST) apparatus. *Water Science and technology* 37.6-7: 117-124.

Meeten, G. H., & Smeulders, J. B. A. F. (1995). Interpretation of filterability measured by the capillary suction time method. *Chemical Engineering Science*, 50(8), 1273-1279.

Rehman Lund, A.A., C.A. Martin, T.K. Gates, J. Scalia IV, M. Munir Babar (2021) Field evaluation of a polymer sealant for canal seepage reduction, *Agricultural Water Management*, 252 <https://doi.org/10.1016/j.agwat.2021.106898>

Rehman Lund, A.A. (2024) Mitigating Canal Seepage: A Great Avenue To Save Irrigation Water, <https://sustainability.colostate.edu/humannature/mitigating-canal-seepage-avenue-to-save-water/> (website bezocht 2024-11-22)

Rijkswaterstaat (2022) Memo Analyse meetdata kanaalafdichting met ZBM, L.A. Zaat, 19-01-2022.

Rijkswaterstaat (2024), A. de Boom, Verificatie effectiviteit ZBM als bodemafdichting op het Twentekanaal.

CIRIA (2007), *The Rock Manual. The use of rock in hydraulic engineering* (second edition).

Soulsby, R. (1997) *Dynamics of Marine Sands*, Publisher Thomas Telford, 1997

Talmon, A. M., Mastbergen, D. R., & Huisman, M. (2013). Invasion of pressurized clay suspensions into granular soil. *Journal of Porous Media*, 16(4).

Talmon, A. M. (2026). Notes on calculation of hydraulic conductivity of sludge from CST test. Personal communication.

Triton Electronics Ltd (2025). Type 304M Mains CST Unit. In <https://www.tritonel.com/shop/304m-type-304m-mains-cst-unit-1377>.

Van Heteren (2020), A. Puls, Beslibbingsonderzoek, versie 3.0 definitief, 24-8-2020.

Witteman, J. (2024), Assessing the hydraulic conductivity of the seepage-reducing measure 'Sand Bentonite' in diverse environments, MSc afstudeerrapport, University of Twente, 3 June 2024.

A Appendix

A.1 Column test data postprocessing

Due to the limited accuracy of the instruments (1 g accuracy, 1 Hz sampling rate), slow filtration rates generate staircase-like artifacts in the timeseries data. This effect is most pronounced during the initial testing phase when the homogeneous, undamaged material resists water leakage. To prevent these 'staircase' patterns from producing noisy or erroneous velocity calculations, a threshold-based algorithm is required to compute slopes over dynamically sized time intervals.

The following algorithm identifies the next immediate point in time j where the average mass accumulation rate (slope) starting from time i exceeds the threshold S . For every data point (m_i, t_i) :

$$z_i = m_i - (S \cdot t_i) \quad (15)$$

For a starting index i , search for the smallest index $j > i$ such that $z_j > z_i$. This inequality is equivalent to:

$$\frac{m_j - m_i}{t_j - t_i} > S \quad (16)$$

The algorithm (eqs.12-13) iterates through the data:

- Start at current index i .
- Find the target j using the logic above.
- Compute filtration velocity and resistance time (eqs.10-11) for the interval $[i, j]$.
- Set the next current index to $j+1$ (skipping all points between i and j).

A.2 Sand – OCMA bentonite CST tests results

Table A.1. The parameters of the tested sand-OCMA bentonite recipes.

	Recipe 1	Recipe 2	Recipe 3
Vol. of Sand (cm³)	195.00	196.00	197.00
Vol. of bentonite (cm³)	5.00	4.00	3.00
Vol. of water (cm³)	200.00	200.00	200.00
Mass of Sand (g)	516.75	519.40	522.05
Mass of bentonite (g)	11.50	9.20	6.90
Mass of water (g)	200.00	200.00	200.00
Volumetric conc. of sand (-)	0.4875	0.4900	0.4925
Volumetric conc. of bentonite (-)	0.0125	0.0100	0.0075
Mass conc. of sand (g/cm³)	1.2919	1.2985	1.3051
Mass conc. of bentonite (g/cm³)	0.0288	0.0230	0.0173

Bulk density (g/cm³)	1.8206	1.8215	1.8224
Average CST (s)	1244.2	728.2	438.9
Hydraulic conductivity (m/s)	1.54E-08	2.64E-08	4.38E-08
Resistance time of a 40 cm layer (day)	300.0	175.6	105.8
Selected for column test	Yes	No	Yes
Column test name	ARK_Base_ourZBM_40cm_high		ARK_Base_ourZBM_40cm_low

A.3 Sand – S1 clay CST test results

Table A.2. The parameters of the tested sand-S1 clay recipes.

	Recipe 1	Recipe 2	Recipe 3
Vol. of sand (cm³)	164.00	168.00	172.00
Vol. of clay (cm³)	36.00	32.00	28.00
Vol. of water (cm³)	200.00	200.00	200.00
Mass of sand (g)	434.60	445.20	455.80
Mass of clay (g)	87.23	77.54	67.84
Mass of water (g)	200.00	200.00	200.00
Volumetric conc. of sand (-)	0.41	0.42	0.43
Volumetric conc. of clay (-)	0.09	0.08	0.07
Mass conc. of sand (g/cm³)	1.0865	1.1130	1.1395
Mass conc. of clay (g/cm³)	0.2181	0.1938	0.1696
Mixture density (g/cm³)	1.8046	1.8068	1.8091
Average CST (s)	417.1	295.6	222.0
Hydraulic conductivity (m/s)	4.60E-08	6.50E-08	8.65E-08
Resistance time of a 40 cm layer (day)	100.5	71.3	53.5
Selected for column test	Yes	No	Yes
Column test name	ARK_Base_ZKM_40cm_high		ARK_Base_ZKM_40cm_low

Table A.3. The parameters of the tested pure S1 clay recipes.

	Recipe 1	Recipe 2	Recipe 3
Vol. of clay (cm ³)	59.66	67.19	70.88
Vol. of water (cm ³)	242.35	235.33	225.00
Mass of clay (g)	144.56	162.80	171.73
Mass of water (g)	242.35	235.33	225.00
Volumetric conc. of clay (-)	0.20	0.22	0.24
Mass conc. of clay (g/cm ³)	0.4787	0.5381	0.5804
Mixture density (g/cm ³)	1.2831	1.3183	1.3409
Average CST (s)	240.7	318.2	421.8
Hydraulic conductivity (m/s)	7.98E-08	6.03E-08	4.55E-08
Resistance time of a 40 cm layer (day)	58.0	76.7	101.7
Selected for column test	No	No	Yes
Column test name			ARK_Base_Clay_10cm_Sand_30cm

A.4 Sand – dredged mud CST test results

Table A.4. The parameters of the tested sand-dredged mud recipes.

	Recipe 1	Recipe 2	Recipe 3	Recipe 4
Vol. of sand (cm ³)	105.00	124.00	143.00	147.75
Vol. of mud (cm ³)	95.00	76.00	57.00	52.25
Vol. of water (cm ³)	200.00	200.00	200.00	200.00
Mass of sand (g)	278.25	328.60	378.95	391.54
Mass of mud (g)	236.55	189.24	141.93	130.10
Mass of water (g)	200.00	200.00	200.00	200.00
Volumetric conc. of sand (-)	0.2625	0.3100	0.3575	0.3694
Volumetric conc. of mud (-)	0.2375	0.1900	0.1425	0.1306
Mass conc. of sand (g/cm ³)	0.6956	0.8215	0.9474	0.9788
Mass conc. of mud (g/cm ³)	0.5914	0.4731	0.3548	0.3253
Mixture density (g/cm ³)	1.7870	1.7946	1.8022	1.8041
Average CST (s)	1248.0	429.7	245.3	194.5
Hydraulic conductivity (m/s)	1.54E-08	4.47E-08	7.83E-08	9.87E-08
Resistance time of a 40 cm layer (day)	300.9	103.6	59.1	46.9

Selected for column test	No	Yes	No	Yes
Column test name		ARK_Base_ZD M_40cm_high		ARK_Base_ZD M_40cm_low

Table A.5. The parameters of the tested pure dredged mud recipes.

	Recipe 1	Recipe 2	Recipe 3	Recipe 4
Vol. of mud (cm³)	95.00	95.00	95.00	95.00
Vol. of water (cm³)	200.00	240.00	260.00	300.00
Mass of mud (g)	236.55	236.55	236.55	236.55
Mass of water (g)	200.00	240.00	260.00	300.00
Volumetric conc. of mud (-)	0.3220	0.2836	0.2676	0.2405
Mass conc. of mud (g/cm³)	0.8019	0.7061	0.6663	0.5989
Mixture density (g/cm³)	1.4798	1.4225	1.3987	1.3584
Average CST (s)	631.9	435.4	361.0	291.7
Hydraulic conductivity (m/s)	3.04E-08	4.41E-08	5.32E-08	6.58E-08
Resistance time of a 40 cm layer (day)	152.3	105.0	87.0	70.3
Selected for column test	No	Yes	No	No
Column test name		ARK_Base_Mud _10cm_Sand_3 0cm		

A.5 Sand – granulite CST test results

Table A.6. The parameters of the tested sand-granulite recipes.

	Recipe 1	Recipe 2	Recipe 3	Recipe 4
Vol. of sand (cm³)	58.95	80.11	97.80	101.27
Vol. of granulite (cm³)	141.05	119.89	102.20	98.74
Vol. of water (cm³)	200.00	200.00	200.00	200.00
Mass of sand (g)	156.22	212.28	259.17	268.35
Mass of granulite (g)	366.73	311.72	265.72	256.71
Mass of water (g)	200.00	200.00	200.00	200.00
Volumetric conc. of sand (-)	0.1474	0.2003	0.2445	0.2532
Volumetric conc. of granulite (-)	0.3526	0.2997	0.2555	0.2468
Mass conc. of sand (g/cm³)	0.3905	0.5307	0.6479	0.6709
Mass conc. of granulite (g/cm³)	0.9168	0.7793	0.6643	0.6418

Mixture density (g/cm³)	1.8074	1.8100	1.8122	1.8127
Average CST (s)	376.1	263.5	215.0	200.7
Hydraulic conductivity (m/s)	5.11E-08	7.29E-08	8.93E-08	9.57E-08
Resistance time of a 40 cm layer (day)	90.7	63.5	51.8	48.4
Selected for column test	Yes	No	No	Yes
Column test name	ARK_Base_ZG M_40cm_high			ARK_Base_ZG M_40cm_low

Deltares is an independent institute for applied research in the field of water and subsurface. Throughout the world, we work on smart solutions for people, environment and society.

Deltares

www.deltares.nl